






Distinct ossification trade-offs illuminate the shoulder girdle reconfiguration at the water-to-land transition

Received: 27 September 2023

Accepted: 14 May 2025

Published online: 29 May 2025



Janet Wei^{1,8}, Thomas W. P. Wood ^{1,8}, Kathleen Flaherty^{2,8}, Olivia E. Fitch³, Shahid Ali⁴, Alyssa Enny¹, Ali Andrescavage¹, Danielle Brazer¹, Dina Navon^{5,6}, Hannah E. Cohen ¹, Derek Gordon¹, Anusha Shanabag¹, Shunya Kuroda ¹, Thomas A. Stewart⁷, Ingo Braasch ³ & Tetsuya Nakamura ¹✉

The mechanisms of the pectoral girdle transformation at the origin of terrestrial locomotion in vertebrates remain an outstanding problem. The loss of intramembranous bones and the enlargement of endochondral bones resulted in the disarticulation of the pectoral girdle from the skull and the formation of the neck during the fish-to-tetrapod transition. Despite the functional implications of this skeletal shift in the emergence of terrestrial vertebrates, the underlying genetic-developmental alterations have remained enigmatic. Here, we show that in zebrafish pectoral girdle mesodermal cells expressing *gli3*, a transcription factor gene in the Hedgehog signaling pathway, differentiate into both intramembranous and endochondral bones. Intriguingly, Gli and Hedgehog compound knockout fish exhibited an unexpected combination of actinopterygian fish and stem-tetrapod pectoral girdle characteristics. These ontogenetic and anatomical data suggest that a trade-off between the two distinct ossification pathways is a deeply embedded developmental program in bony fishes and that tuning of this trade-off can generate novel pectoral girdle akin to those of stem-tetrapods at the dawn of vertebrate terrestrialization.

Across the fish-to-tetrapod transition, the amount of intramembranous (direct ossification of mesenchyme) bones decreased and that of endochondral bones (ossification replacing a cartilage template) increased throughout the vertebrate body, facilitating terrestrial feeding, locomotion, and breathing^{1–4}. The pectoral, or shoulder, girdle is a dramatic example of this intramembranous-to-endochondral skeletal shift. In bony ray-finned (actinopterygian) and lobe-finned (sarcopterygian) fishes, the pectoral girdle consists of a relatively small

endochondral component (scapula and coracoid bones) and a large series of intramembranous bones (i.e., cleithrum, clavicle, and supra-cleithrum) that link the scapula and coracoid to the skull⁵ (Fig. 1a). As vertebrates transitioned onto land in the Late Devonian, the scapula and coracoid expanded, serving as robust attachment sites of forelimb musculature for terrestrial locomotion^{6–8}. Concomitantly, a reduction of the intramembranous bones disconnected the pectoral girdle from the skull and triggered the evolution of a functional neck, providing

¹Department of Genetics, Rutgers the State University of New Jersey, Piscataway, NJ, USA. ²Comparative Medicine Resources, Rutgers the State University of New Jersey, Piscataway, NJ, USA. ³Department of Integrative Biology and Ecology, Evolution, and Behavior Program, Michigan State University, East Lansing, MI, USA. ⁴Department of Organismal Biology and Anatomy, University of Chicago, Chicago, IL, USA. ⁵Pathology Department, INSPIRE Program, Robert Wood Johnson Medical School, New Brunswick, NJ, USA. ⁶Biology Department, University of the Fraser Valley, Abbotsford, BC, Canada. ⁷Department of Biology, The Pennsylvania State University, University Park, Pennsylvania, PA, USA. ⁸These authors contributed equally: Janet Wei, Thomas W. P. Wood, Kathleen Flaherty. ✉e-mail: nakamura@dls.rutgers.edu

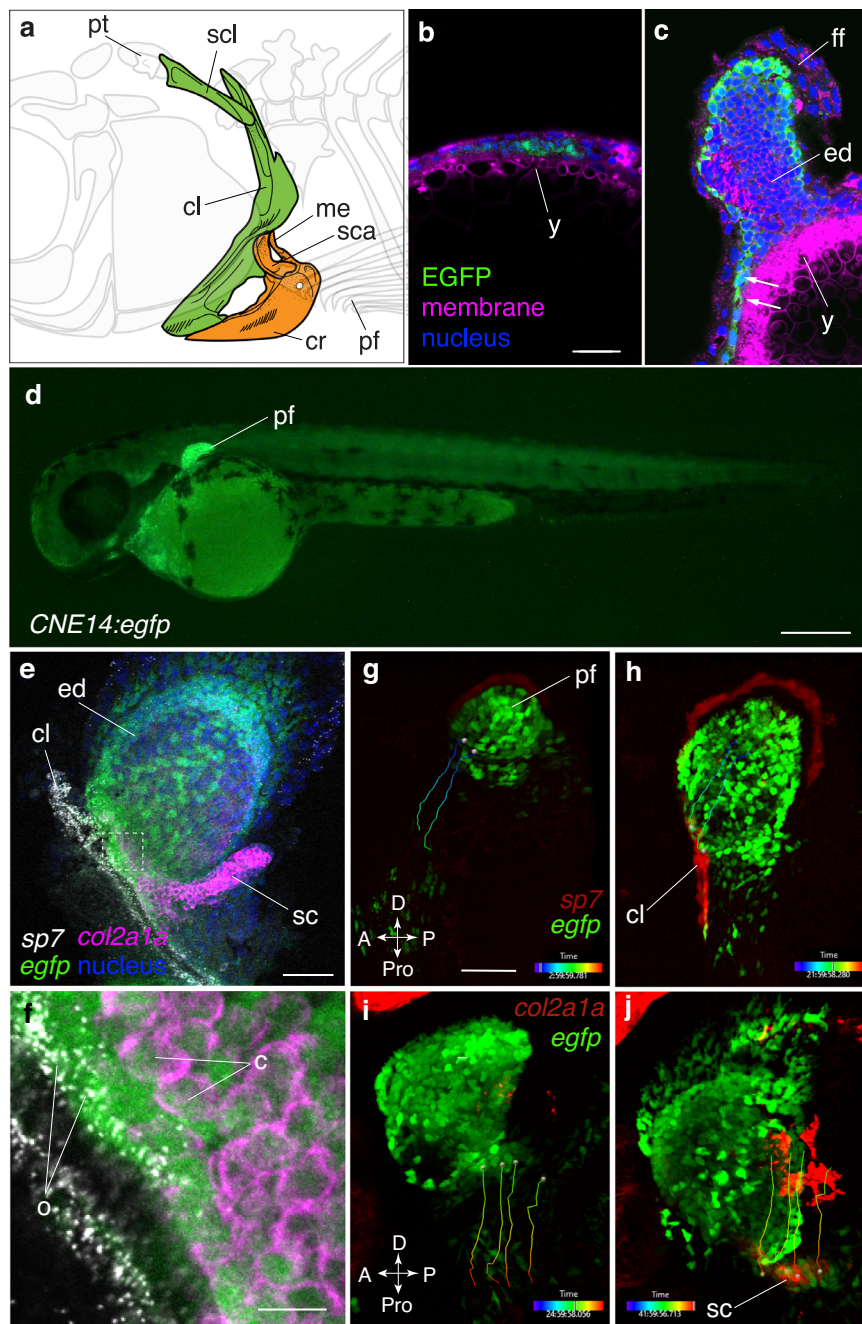


Fig. 1 | *Gli3*-positive cells contribute to the cleithrum and the scapulocoracoid in the pectoral girdle. **a** The adult zebrafish pectoral girdle bones. The intramembranous bones and endochondral bones are highlighted by green and orange, respectively. The intramembranous series is connected to the posterior skull via the post-temporal bone (pt). The pectoral fin (pf) articulates on the scapula (sca). cr, coracoid; cl, cleithrum; me, mesocoracoid; scl, supracleithrum. **b, c** Digitally sectioned immunofluorescence of EGFP with membrane (CellMask) and nucleus (DAPI) staining of *CNE14:egfp* embryos at 32 hpf (**b**) and 48 hpf (**c**). Bright EGFP expression is observed in the mesenchymal cells at the prospective pectoral fin region at 32 hpf. As the pectoral fin grows, EGFP-positive cells are localized in the fin mesenchyme, including the proximal fin, at 48 hpf. These images were 3D-digital sections obtained by a confocal microscope and at the same scale. **n** = 12. **d** A stereotyped fluorescent microscope image of *CNE14:egfp* transgenic embryo at 48 hpf. The transgenic embryos exhibit bright EGFP expression in the pectoral fin. **n** = 49. **e, f** HCR of *CNE14:egfp* pectoral fin region with probes complementary to *col2a1a* for chondrocytes (scapulocoracoid “sc”, magenta), *sp7* for osteoblasts (“cl”, white), and *egfp* (*gli3*-positive cells, green) with DAPI staining (nuclei, blue) at 72 hpf. **n** = 19

(See Supplementary Tables 5–7). **f** The enlarged image of the proximal pectoral fin marked by the rectangle in **e**. *Egfp*-positive cells express *col2a1a* in the scapulocoracoid and *sp7* in the cleithrum, indicating that *gli3*-positive cells differentiate into proliferating chondrocytes and osteoblasts. **n** = 23. **g–j** Live fluorescent imaging of the pectoral fin in *CNE14:egfp; sp7:mCherry* (**g** and **h**) or *CNE14:egfp; col2a1aBAC:mCherry* (**i**, **j**) embryo from 32 to 74 hpf. The shown images are representative 3D projections at 35 hpf (**g**), 54 hpf (**h**), 56 hpf (**i**), and 74 hpf (**j**). Images in **g–j** were generated by Imaris (Method). The prospective scapulocoracoid and cleithrum cells reside inside or proximal to the pectoral fin (**g**, **i**). These cells migrate proximally and form pectoral girdle bones as development proceeds (**h**, **j**). Cell migration trajectories are dragon tails created by Imaris. The unit of the time bars is hours. **n** = 3. The images in (**g–j**) are at the same scale. EGFP-positive cells contribute to the endochondral disc (ed), the scapulocoracoid (sc), and the cleithrum (cl). Scale bars are 20 μ m (**b**), 300 μ m (**d**), 50 μ m (**e**, **i**), and 500 μ m (**j**). A anterior, P posterior, D distal, and Pro proximal, c chondrocytes, cl cleithrum, ed endochondral disc, ff fin fold, o osteoblast, pf pectoral fin, sc scapulocoracoid, and y yolk.

greater mobility to the head⁹. Despite the profound functional implications of this intramembranous-to-endochondral shift in the pectoral girdle of early tetrapods, the underlying genetic and developmental changes of this evolutionary transformation remain unexplored.

It was long hypothesized that these two bone types arose from distinct cell populations. Intramembranous bones were proposed to develop from neural crest cells, whereas endochondral bones were thought to develop from mesodermal cells¹⁰. However, recent studies have challenged this paradigm and provided evidence that the two distinct ossification modes could share common developmental origins in tetrapods^{11–13}. For example, in chicken and mouse embryos, the clavicle develops via intramembranous ossification from the lateral plate mesoderm (LPM) cells and cardiopharyngeal mesoderm (CPM)^{14–18}. Additionally, the scapula, which is endoskeletal, originates as an admixture of the LPM and the paraxial mesoderm (PAM) cells in mice, chicken, axolotls, and, tentatively, in turtles^{19–24}. A previous study in mice suggested that neural crest cells also contribute to the muscle attachment site of the scapula²⁵. Because it was assumed that the cleithrum of actinopterygian fishes has a neural crest origin, it was hypothesized that the neural crest contribution to the scapula is a remnant of the lost cleithrum—“the cleithrum’s ghost”²⁵. Neural crest contribution to the scapula, however, has not been detected in other studies in tetrapods^{18,25,26}, and, thus, is still under debate. Intriguingly, a recent study discovered that the zebrafish (*Danio rerio*) cleithrum develops from four distinct embryonic cell populations (neural crest, CPM, LPM, and PAM), while the scapula develops solely from LPM²⁷. This knowledge illuminates how the compositional changes in the embryonic origins contributed to the shift from intramembranous to endochondral bones in the pectoral girdle during the fish-to-tetrapod transition. Yet taxonomically broad investigations of pectoral girdle embryonic origins in other vertebrates with paired fins (chondrichthyan, actinopterygian, and sarcopterygian fishes except for tetrapods) would answer how tetrapod intramembranous and endochondral bones obtained common developmental origins.

Zebrafish belong to Ostariophysan clade, which is one of the largest groups in actinopterygian fishes and includes 28% of extant teleost fishes²⁸. Zebrafish are a prominent fish model system for dissecting the molecular mechanisms underlying skeletal development due to its superb amiability to genetic approaches. *D. rerio* also represent a powerful model for analyzing pectoral girdle evolution in early tetrapods; zebrafish exhibit numerous evolutionarily conserved anatomical features of their girdle that are seen in basal sarcopterygian fishes and stem-tetrapods, including the cleithrum, supracleithrum, coracoid, scapula, mesocoracoid, and supracleithrum except for anocleithrum^{8,29,30}. Some ossification processes of teleost and basal actinopterygian fishes, however, differ from that of tetrapods, for example, many bones conventionally called endochondral bones, including pectoral fins and girdle, use perichondral ossification during early embryonic development in teleosts^{31–34}. Also, miniaturization of teleosts fishes altered ossification modes, bone structures, and morphology^{35–38}. Despite these ontogenetic and structural difference, the genes indispensable for osteoblast and chondrocyte differentiation are tightly conserved between actinopterygians and tetrapods³⁹. These findings make zebrafish a compelling model to scrutinize the ossification molecular mechanisms in ray-finned fishes and to illuminate the water-to-land transition.

Limited knowledge about the genetic pathways responsible for pectoral girdle formation of vertebrates with paired fins represents a major obstacle to discovering the molecular mechanisms responsible for the evolution of the terrestrial pectoral girdle over the course of the fish-to-tetrapod transition. In mice, the *Pbx* genes, which encode TALE homeoprotein transcription factors, play pivotal roles in endochondral acromion and scapular blade formation, inducing the expression of various transcription factor genes, such as *Alx1*, *Tbx15*, *Gli3*, and *Pax1*^{40–43}. Additionally, *Tbx5*^{−/−} mice exhibit a loss of the entire scapula⁴⁴.

In contrast to the accumulated knowledge of the genetic mechanisms required for mammalian and avian pectoral girdle formation, the knowledge of genes involved in fish pectoral girdle formation is limited to only a few studies^{45–48}.

Gli gene products belong to the Kruppel family of zinc finger protein family and show a profound evolutionarily conservation across invertebrates and vertebrates^{49,50}. Mechanistically, Gli proteins are components of the Hedgehog (Hh) - Gli signaling pathway, where they function as a transcriptional activator upon the binding of Hh ligands to Patched (Ptch) membrane receptors or as a transcriptional repressors without Hh ligands⁵¹. Gli proteins are indispensable for animal body development and homeostasis. Coding sequence mutations or large genome deletions at the human *GLI3* locus, one of the *GLI* family genes cause congenital skeletal diseases, including Greig cephalopolysyndactyly characterized by macrocephaly, preaxial polydactyly, intellectual disability, and other severe phenotypes⁵². GLI3-related Pallister-Hall syndromes (PHS) is another congenital disease paired with hypothalamic hamartoma and mesoaxial polydactyly⁵³. Yet the evolutionary conservation of Gli3 functions during the ontogeny of the aquatic fish body remains largely undetermined.

Previous studies showed that Gli3 plays a key regulatory role in shoulder girdle formation as well as in the patterning of distal appendages in tetrapods^{54–56}, making *gli3* a compelling candidate gene for understanding the development of the pectoral girdle in fishes. In limb development, *Gli3* is expressed in the anterior limb bud as compared to the posteriorly localized *Sonic hedgehog* (*Shh*) expression and, thus, is mostly processed to the repressor form without Hh ligands⁵⁵. *Gli3* deletion in mice causes a wide scapula blade and polydactyly, demonstrating that the GLI3 repressor restricts scapula width and digit number^{41,55,57,58}. Deletion of *gli3* in the teleost fish medaka further supports the notion that it has an evolutionary conserved function in repressing fin ray and endochondral bone number in the pectoral fin⁵⁹. Moreover, the previous studies demonstrated that *shha* (one of the *shh* genes created in the teleost-specific whole genome duplication (TGD⁶⁰)) is indispensable for the formation of the cleithrum and the scapulocoracoid, a primordium of the scapula and coracoid, in the zebrafish and medaka pectoral girdles^{61,62}. However, further investigation of Hh-Gli signaling is crucial to elucidate the genetic mechanisms of intramembranous and endochondral bone specification and development in vertebrates with paired fins.

In this study, we investigated the functions of Hh-Gli signaling in zebrafish pectoral girdle development with an emphasis on the balancing mechanism of intramembranous and endochondral ossification. In addition, by conducting the unbiased genomic screening, we identified the downstream target genes of the Hh-Gli signaling, including *activin A receptor type 1-like* (*acrv1l*). These newly obtained results suggest that changes in the Hh-Gli signaling or its associated genes might have contributed to the transformation of the pectoral girdle during the water-to-land transition.

Results

Contribution of *gli3*-positive cells to intramembranous and endochondral pectoral girdle bones

To identify the embryonic origins of the two types of ossification in the pectoral girdle of vertebrates with paired fins, we genetically mapped the contribution of *gli3*-positive cells, which are of lateral plate mesoderm origin in tetrapods^{58,63–65}, to pectoral girdle bones using the zebrafish transgenic system. We conducted an evolutionary sequence comparison of conserved noncoding element 14 (*CNE14*), a *gli3* enhancer for pectoral appendage expression⁵⁸ among the ray-finned zebrafish and spotted gar, the chondrichthyan elephant shark, and tetrapod Western clawed frog, mouse, and human (Supplementary Fig. 1). *CNE14* is highly conserved among these species, except for zebrafish, which showed a lower conservation compared to other species. Next, we cloned both zebrafish and elephant shark *CNE14*

upstream of a basal promoter and EGFP and tested their activities by injecting them into fertilized zebrafish eggs (see Methods section). Intriguingly, while zebrafish *CNE14* did not show EGFP expression in the pectoral fin, elephant shark *CNE14* showed conspicuously fin-localized EGFP fluorescence from 32 h post-fertilization (hpf) and beyond (Fig. 1b–d, and Supplementary Fig. 1). Chondrichthyans have not undergone the TGD, and we therefore regard the conspicuous fin-localized activity produced by the elephant shark enhancer as most likely due to a retention of an evolutionarily conserved *cis*-regulatory sequence and activity that would have been plesiomorphic to gnathostomes⁶⁶. Next, we established elephant shark *CNE14:egfp* transgenic zebrafish (hereafter “*CNE14:egfp*”). Using multiplexed fluorescent in situ hybridization chain reaction (HCR), we confirmed that *CNE14:egfp* fluorescence marks the endogenous *gli3*-positive mesenchymal cells in the entire endochondral disc and, therefore, is a practical reporter of *gli3*-positive cells (Supplementary Fig. 1).

To determine whether *gli3*-positive cells contribute to the two distinct types of ossification, we conducted HCR with probes complementary to *egfp* (*gli3*-positive cells) and *sp7* (osteoblast marker⁶⁷) or *col2a1a* (proliferative chondrocyte marker⁶⁸) using *CNE14:egfp* transgenic embryos. We found that EGFP-positive cells express *sp7* in the cleithrum and *col2a1a* in the scapulocoracoid at 72 hpf (Fig. 1e, f). To further validate whether *gli3*-positive cells differentiate into osteoblasts or chondrocytes in the pectoral girdle, we performed fluorescent live-cell imaging of *CNE14:egfp; sp7:mCherry*⁶⁹ and *CNE14:egfp; col2a1aBAC:mCherry-NTR*⁷⁰ fish using a confocal microscope with a temperature and humidity control from 32 to 74 hpf. This live imaging and subsequent 3D cell migration analysis showed that EGFP-positive cells inside and peripheral to the proximal pectoral fin at 32 hpf migrate to proximal direction and start express *mCherry* driven by *sp7* enhancer in the cleithrum at 55 hpf or *mCherry* driven by the *col2a1a* BAC in the scapulocoracoid at 63 hpf (Fig. 1g–j). Taken together, these results demonstrate that *gli3*-positive cells inside and peripheral to the early fin bud migrate and differentiate to osteoblasts in the cleithrum or chondrocytes in the scapulocoracoid in zebrafish embryos.

Morphological phenotype of *gli3* knockout zebrafish

To test the function of Gli3 in zebrafish ossification, we generated stable *gli3* homozygous knockout zebrafish mutants bearing a frameshift mutation in exon5 (*gli3*^{14ins/14ins}) using CRISPR/Cas9 (Supplementary Fig. 2 and Supplementary Table 1). At 7 and 30 days post fertilization (dpf), gross observation indicated that *gli3*^{14ins/14ins} fish possess the normal body morphology, including the eye, yolk, median fin fold, and cloaca (Supplementary Fig. 3). We also conducted acid-free skeletal staining of 13 and 30 dpf juveniles and did not find significant difference in ossification of cranial, trunk, and tail skeletons, including the opercular, parashenoid, vertebrae, and hypural bones between wildtype and *gli3*^{14ins/14ins} fish. The dorsal extension of the cleithrum, however, is slightly shorter than that of wildtype in some *gli3*^{14ins/14ins} juveniles ($n = 2/8$, Supplementary Fig. 3). Survival of *gli3*^{14ins/14ins} fish to adulthood allowed us to determine the functional roles of the Hh-Gli signaling pathway in adult body structures (Supplementary Fig. 4). Gross observation indicated that some adult *gli3*^{14ins/14ins} fish possess an external notch posterior to the jaw bones (Supplementary Fig. 4, 28/159). We then scrutinized alterations of skeletal morphology throughout the body of adult *gli3*^{14ins/14ins} fish using bone and cartilage staining followed by dissections (Methods, Supplementary Figs. 4–6). Compared to wildtype fish, *gli3*^{14ins/14ins} fish showed excessively mineralized skull bones, including of the parietal and frontal bones, and ectopic ossification in the eye lens at 3 months-old (Supplementary Fig. 4, $n = 5/7$). The excessive mineralization phenotype matches GLI3-related human congenital diseases, such as Greig cephalopolysyndactyly and Pallister-Hall syndromes^{52,71}. Moreover, *gli3*^{14ins/14ins} zebrafish exhibited an abnormally expanded telencephalon at three months old (Supplementary Fig. 7, Supplementary Table 3).

Intriguingly, we did not find any increase of fin ray or endochondral radial numbers in the pectoral fin as previously observed in *gli3* knockout medaka fish (Supplementary Table 4)⁷². The lack of ossification phenotype in *gli3*^{14ins/14ins} pectoral fin is consistent with another independent study that generated *gli3* knockout zebrafish with a different genetic mutation⁷³.

Gli3 determines the balance of osteoblast and chondrocyte differentiation

Next, to analyze the function of Gli3 in the intramembranous and endochondral ossification of the pectoral girdle, we conducted HCR with probes complementary to *sp7* and *col2a1a* using *gli3*^{14ins/14ins} embryos. The quantification of *sp7*-positive cells showed that fewer osteoblasts are present in the cleithrum at the level of the scapulocoracoid in *gli3*^{14ins/14ins} mutants compared to wildtype embryos at 72 hpf (Fig. 2a and b, Supplementary Table 5–7, $p = 0.00018$). We also compared *sp7:egfp* expression in the cleithrum of wildtype and *gli3*^{14ins/14ins} embryos. EGFP expression is weaker in the ventral part of the cleithrum in *gli3*^{14ins/14ins} embryos than wildtype (Supplementary Fig. 8). Gli3 functions as a transcriptional activator or repressor depending on the presence of Hh²⁸. Therefore, osteoblast reduction could arise from a loss of either or both functions. To differentiate between these possibilities, we treated wildtype zebrafish embryos with BMS-833923, a Smoothed antagonist (i.e., Hedgehog inhibitor⁷⁴) that decreases the amount of Gli activator from 32 hpf to 72 hpf. In BMS-833923-treated embryos, we observed fewer osteoblasts in the cleithrum at the level of the scapulocoracoid than wildtype embryos in a comparable manner to *gli3*^{14ins/14ins} embryos at the equivalent total body length stage (wildtype embryos at 68 hpf and BMS-833923-treated embryos at 72 hpf embryos, $p = 0.0028$) (Supplementary Fig. 9, Supplementary Table 5–7). This demonstrates the functional significance of the Gli activator in osteoblast differentiation in the cleithrum.

To genetically corroborate that Gli functions as an activator in the zebrafish pectoral girdle, we decreased the amount of Gli activator by introducing a stable frameshift mutation into the coding sequence of *gli2b*, encoding another Gli family zinc finger protein that mainly functions as a transcriptional activator⁵⁰, in *gli3*^{14ins/14ins} embryos using CRISPR/Cas9 (Supplementary Fig. 2, Supplementary Table 1). Consistent with the phenotype of BMS-833923-treated embryos, *gli2b*^{17ins/17ins}; *gli3*^{14ins/14ins} double knockout embryos have fewer osteoblasts in the cleithrum at the position where the scapulocoracoid attaches than *gli3*^{14ins/14ins} embryos at 72 hpf (Fig. 2c, Supplementary Tables 5, 6, average number; 23.6 cells in *gli3*^{14ins/14ins} vs 16.77 cells in *gli2b*^{17ins/17ins}; *gli3*^{14ins/14ins} embryos). However, an ANOVA test did not detect a statistically significant difference between these two genotypes ($p = 0.12$, Supplementary Table 7). Intriguingly, we also observed that the number of *col2a1a*-positive proliferative chondrocytes in the scapulocoracoid of *gli3*^{14ins/14ins} embryos increased compared to wildtype embryos (Fig. 2f, g and Supplementary Fig. 10, Supplementary Table 7, $p = 0.0000178$). Albeit the difference of averaged chondrocyte numbers between in wildtype and *gli2b*^{17ins/17ins}; *gli3*^{14ins/14ins} embryos (165.67 vs 193.69, Supplementary Table 5), we did not detect a statistically significant difference between them ($p = 0.06$). These results suggest that the Gli3 activator form, and possibly Gli2b with a relatively weak contribution, induces osteoblast differentiation in the cleithrum at the expense of chondrocytes in the scapulocoracoid.

Regulation of BMP signaling via *activin A receptor type 1-like* expression by Gli3

To elucidate the Gli3 pathway that determines osteoblast and chondrocyte differentiation, we identified Gli3 target genes in an unbiased way by combining RNA-sequencing (RNA-seq) and Assay for Transposase-Accessible Chromatin using sequencing (ATAC-seq) in wildtype and *gli3*^{14ins/14ins} embryos (Fig. 3a). We separately isolated

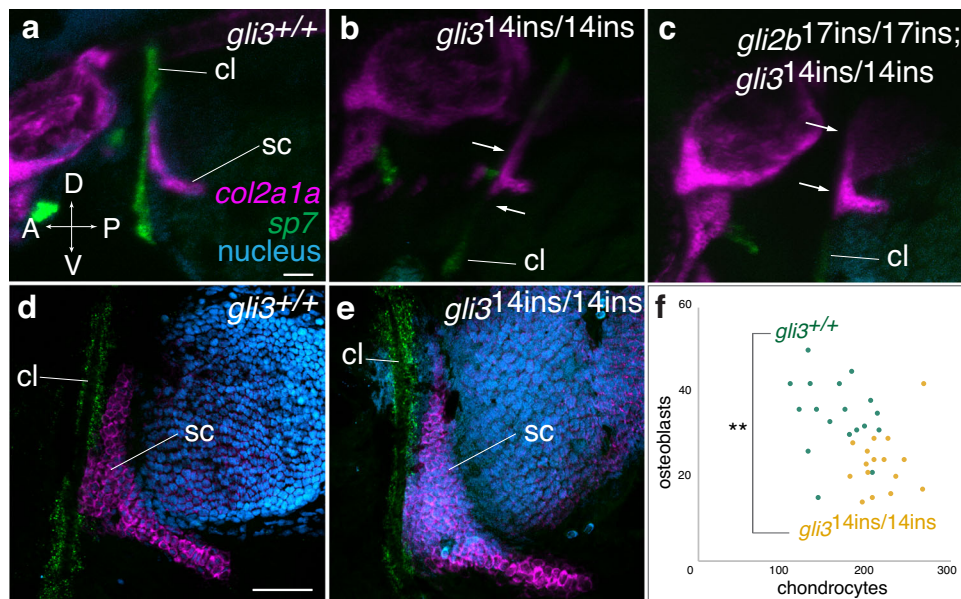


Fig. 2 | The trade-off of osteoblast and chondrocyte differentiation regulated by *gli* genes. a–c HCR of *col2a1a* (magenta) and *sp7* (green) with DAPI staining (cyan). 3D stack lateral visualization of confocal scanning of *gli3*^{+/+} (a), *gli3*^{14ins/14ins} (b), and *gli2b*^{17ins/17ins}; *gli3*^{14ins/14ins} embryos (c). The osteoblasts around the cleithrum at the level of the scapulocoracoid are reduced in *gli3*^{14ins/14ins} and *gli2b*^{17ins/17ins}; *gli3*^{14ins/14ins} embryos (b, c). *n* = 6 for each genotype. The scales are the same from (a–c). **d, e** Dissected pectoral fins of *gli3*^{+/+} (d) and *gli3*^{14ins/14ins} (e) embryos at 72 hpf

after HCR with the same probes used in (a–c). The scapulocoracoid is larger in *gli3*^{14ins/14ins} embryos (e) than in *gli3*^{+/+} embryos (d). The scale is the same between (d, e). **f** The comparison of the osteoblast (*sp7*-positive) and chondrocyte (*col2a1a*-positive) numbers in the cleithrum and the scapulocoracoid, respectively, between *gli3*^{+/+} and *gli3*^{14ins/14ins} embryos (*n* = 18 for *gli3*^{+/+} and *n* = 16 for *gli3*^{14ins/14ins} embryos). **, *p* = 0.0000178 by a two-tailed student *t*-test. Scale bars are 300 μm in (a) and 50 μm in (d). cl cleithrum, sc scapulocoracoid.

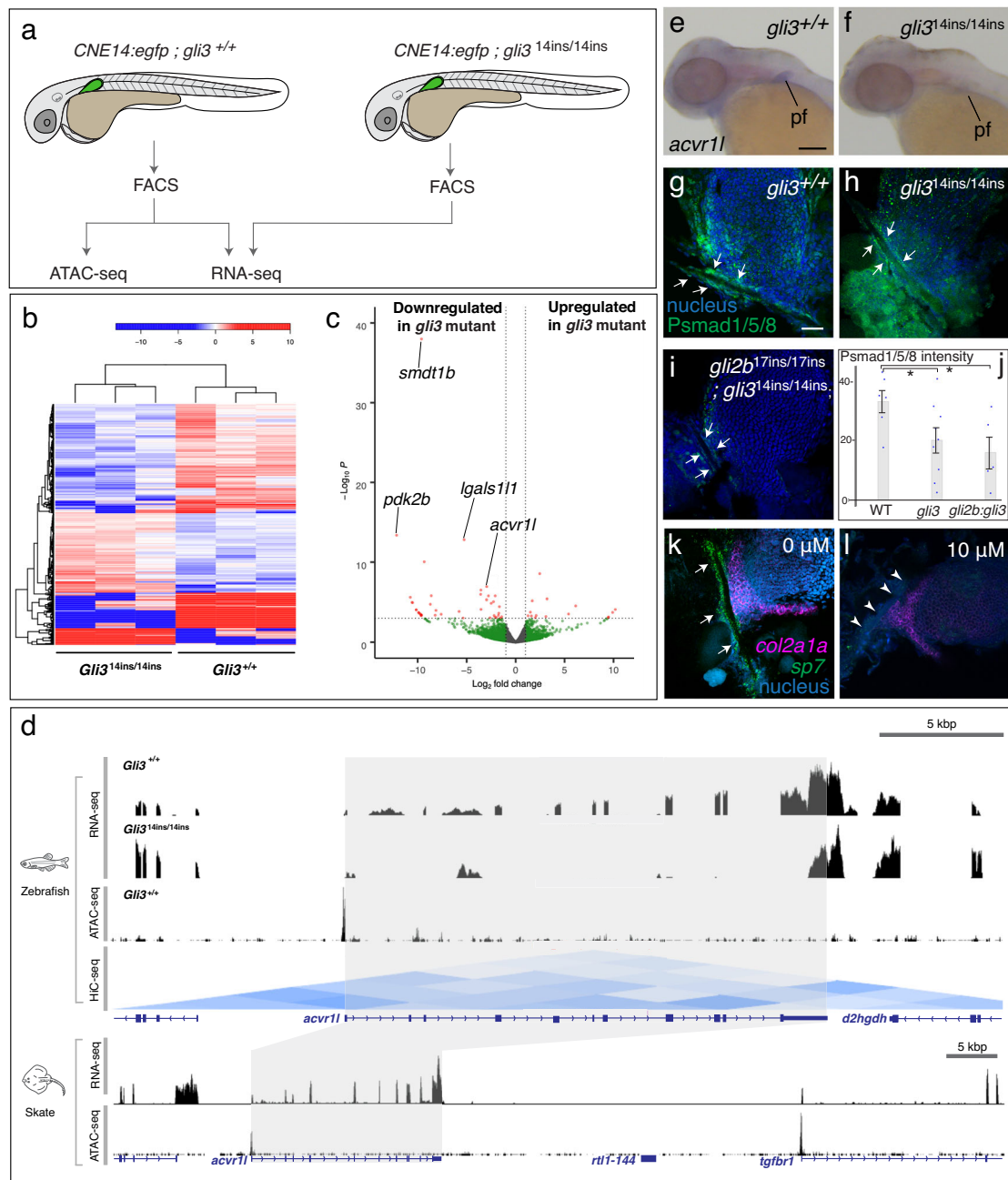
EGFP-positive cells from *CNE14:egfp*; *gli3*^{+/+} and *CNE14:egfp*; *gli3*^{14ins/14ins} embryos by Fluorescence Activated Cell Sorting (FACS) and conducted RNA-seq at 55hpf, when both the cleithrum and the scapulocoracoid are at their early developmental stages (Fig. 3a). A comparative analysis of transcriptome profiles between EGFP-positive cells in *gli3*^{+/+} and *gli3*^{14ins/14ins} embryos identified 351 significantly upregulated genes and 232 downregulated genes (*p* < 0.05) (Fig. 3b, Supplementary Data 1). This gene list includes *klf3* and *zic3*, which were previously identified as direct GLI3 target genes in mouse limb buds⁷⁵, supporting the efficacy of our method. Next, we conducted ATAC-seq with EGFP-positive cells sorted from *CNE14:egfp*; *gli3*^{+/+} embryos at 55 hpf, identified accessible chromatin regions (ACRs) in a genome-wide manner, and annotated these ACRs to genes depending on the proximity to transcription start sites (Supplementary Data 2). The gene with one of the lowest *p*-values from RNA-seq and an ACR promoter is *activin A receptor type 1-like* (*acvr1l*), which encodes a BMP receptor type I⁷⁶ (Fig. 3c). Given the necessity of BMP signaling in osteoblast and chondrocyte differentiation and its involvement in human skeletal diseases^{77–80}, zebrafish *acvr1l* is a compelling Gli3 target for pectoral girdle development. An analysis of previously published Hi-C data indicates that the *acvr1l* promoter domain is in a ~90 kbp topologically associating domain (TAD), suggesting its *cis*-regulatory elements lie in this region⁸¹ (Fig. 3d). Intriguingly, our analysis of the *Activin receptor 1* gene family history indicated that the *Acvr1l* gene is evolutionarily conserved in all extant jawed fish lineages yet got lost multiple times independently in the major extant tetrapod lineages (Supplementary Fig. 11). The notable exception are crocodilians that retained *Acvr1l*. We therefore propose that the functional importance of the *Acvr1l* gene gradually faded in tetrapods, concomitantly with the intramembranous-to-endochondral skeletal shift of the pectoral girdle starting during the fish-to-tetrapod transition (Supplementary Fig. 11, Supplementary Table 8, and Supplementary Note 1).

Subsequent whole-mount RNA in situ hybridization corroborated the regulation of *acvr1l* by Gli3; *acvr1l* transcripts are enriched in the endochondral disc of the wildtype pectoral fin but are decreased in

gli3^{14ins/14ins} fin at 55 hpf (Fig. 3e, f). Moreover, we found *acvr1l* expression in the pectoral fin is a shared feature with chondrichthyans (little skate, *Leucoraja erinacea*) and non-teleost actinopterygians (spotted gar, *Lepisosteus oculatus*) (Supplementary Fig. 12). In accordance with the reduction of *acvr1l* expression in *gli3*^{14ins/14ins} zebrafish embryos, we also found a significant decrease in staining levels of phosphorylated Smad1/5/8 (the active form of Smad1/5/8 in BMP signaling) in osteoblasts surrounding the cleithrum bone from wildtype to *gli3*^{14ins/14ins} embryos (*p* = 0.02), and possibly to *gli2b*^{17ins/17ins}; *gli3*^{14ins/14ins} embryos but not at a statistically significant level (*p* = 0.28) (Fig. 3g–i, Supplementary Table 9). This may reflect a relatively weak function of Gli2b compared to Gli3 in pectoral girdle development. Finally, to test the function of *Acvr1l* in the differentiation of osteoblasts and chondrocytes in shoulder girdle formation, we treated wildtype zebrafish embryos with an Activin receptor type 1 inhibitor LDN193189⁸² from 32 to 72 hpf. Compared to the proper expression of *sp7* and *col2a1a* in the control pectoral girdle, *sp7* expression was diminished in LDN193189-treated embryos (Fig. 3k, l). Therefore, the differentiation of osteoblasts requires BMP signaling via *Acvr1l* in the fish pectoral girdle.

Hedgehog-Gli mutant zebrafish recapitulate evolutionary trajectories of intramembranous and endochondral bones along the water-to-land axis

The pectoral girdle in non-teleost actinopterygians consists of a series of intramembranous (supracleithrum, cleithrum, and clavicle) and endochondral bones (scapulocoracoid and mesocoracoid)⁸³. Teleosts, including zebrafish, share these fundamental components, except for the separation of the scapula and coracoid and the loss of the clavicles⁸⁴ (Fig. 4a). Gross examination and skeletal staining showed that in approximately 20 % of *gli3*^{14ins/14ins} zebrafish either the left or right pectoral fin shifted dorsally due to the dorsoventrally shortened cleithrum (28/159 fish, Supplementary Fig. 4). Intriguingly, subsequent μCT scanning and three-dimensional morphometric analysis revealed mixed characteristics of actinopterygian and stem-tetrapodomorph pectoral girdle morphologies in these severely affected girdles; the



dorsal blade of the cleithrum and the posterior branchial lamina, which posteriorly supports opercular chamber movement in fish, were markedly reduced (Fig. 4a, d, j, Supplementary Fig. 13 and Supplementary Data 3). Moreover, the supracleithrum was absent (Fig. 4a, d, Supplementary Fig. 4), resembling the condition of stem-tetrapods such as *Tulerpeton*^{7,85}. The cleithrum on the opposite side in these severely affected fish and on both sides in the remaining 80% of *gli3^{14ins/14ins}* zebrafish was dorsoventrally shorter compared to those of wildtype individuals (Supplementary Fig. 14, Supplementary Data 3, $n = 23/23$). In addition to the reduction of the intramembranous series, the scapula of *gli3^{14ins/14ins}* zebrafish exhibited the characteristics of stem-tetrapod traits; an enlarged supraglenoid buttress and the antero-medially extended flange for the glenoid (Fig. 4b, e). The glenoid was ovoid and concave in *gli3^{14ins/14ins}* fish, and it is posterolaterally opened compared to the flat glenoid in wildtype fish (Fig. 4b, c, e, f; $n = 3/6$).

The mesocoracoid is another endochondral bone that bridges the coracoid and the cleithrum and is present in actinopterygian fishes but not in sarcopterygian fishes or stem-tetrapods such as *Tiktaalik* or

Acanthostega. In these stem-tetrapods, the supraglenoid buttress is the evolutionary counterpart of the mesocoracoid⁸⁶. The mesocoracoid/supraglenoid buttress becomes stouter from fishes with paired fins to stem-tetrapods to serve as an attachment site for the dorso-medial musculature of the forelimb⁸⁷. In *gli3^{14ins/14ins}* zebrafish, the mesocoracoid is laterally wider than in the wildtype (Fig. 4c, f, $n = 4/5$).

Additionally, to investigate whether the pectoral girdle phenotype is exacerbated by a further reduction of Gli activator, we injected gRNA complementary to zebrafish *shha* with *Cas9* mRNA into *gli3^{14ins/14ins}* eggs, raised them for 3 months, and genotyped them by deep sequencing of *shha* (see Methods). Strikingly, *gli3^{14ins/14ins}; shha^{30%}* fish (30% of the intact *shha* is detected) exhibited a dorsoventrally short cleithrum comparable to the severely affected cleithrum in *gli3^{14ins/14ins}* fish, but on both the left and right sides (Fig. 4g, $n = 3/3$). The shape of the scapula in this compound knockout fish is also concave and posterolaterally opened (Fig. 4h, i). *gli3^{14ins/14ins}; shha^{30%}* fish also showed smaller ratio of cleithrum/scapulocoracoid volume than those of wildtype fish (Supplementary Fig. 15 and Supplementary Data 4). These

Fig. 3 | Gli genes regulate BMP signaling via *activin receptor type 1-like* expression. **a** The experimental scheme of the unbiased high-throughput genomic screening (see Methods). From *CNE14:egfp; gli3^{+/+}* and *CNE14:egfp; gli3^{4ins/14ins}* embryos, EGFP-positive cells were separately isolated by FACS. The sorted cells were subjected to RNA-seq and ATAC-seq. Three biological replicates were conducted for RNA-sequencing and two were for ATAC-seq. **b** The heat map of top 2000 differentially expressed genes in *CNE14:egfp; gli3^{+/+}* and *CNE14:egfp; gli3^{4ins/14ins}* embryos. Color code: red indicates high and blue indicates low enrichment. **c** The volcano plot of the RNA-seq result. The genes with $p < 0.5$ and > 2 -fold expression change are coded by red. The genes on the left side (Log_2 fold change < 0) are down-regulated genes in *gli3^{4ins/14ins}* embryos while the genes on the right side (Log_2 fold change > 0) are up-regulated genes in the mutant embryos. *Acrv11* is one of the prominent Gli3 candidate genes. The statistical analysis was conducted by EdgeR program. **d** The genome browser visualization of zebrafish RNA-seq (wildtype and *gli3^{4ins/14ins}* samples), ATAC-seq, and HiC results, and skate RNA-seq and ATAC-seq results at the *acrv11* locus. In zebrafish, the transcript level is lower at the exons of *acrv11* in *gli3^{4ins/14ins}* embryos than *gli3^{+/+}* embryos. Zebrafish ATAC-seq and HiC showed that the promoter region of *acrv11* is ACR and in a TAD. Zebrafish HiC result was produced from the previously published data³¹. Skate RNA-seq and ATAC-seq data were generated from the previous paper¹¹⁸. **e, f** The expression pattern of *acrv11* in *gli3^{+/+}* and *gli3^{4ins/14ins}* embryos. Expression in the pectoral fin is decreased

in *gli3^{4ins/14ins}* embryos compared to *gli3^{+/+}* embryos. $n = 24$. The scale is the same in (e, f). **g–i** Immunofluorescence of phosphorylated-Smad 1/5/8. The strong signal is observed in cells surrounding the cleithrum of wildtype embryos (**g**, arrows), which decreases to *gli3^{4ins/14ins}* (**h**) and to *gli2b^{17ins/17ins}; gli3^{4ins/14ins}* embryos (**i**). $n = 6$ for wildtype, 9 for *gli3^{4ins/14ins}*, and 5 for *gli2b^{17ins/17ins}; gli3^{4ins/14ins}* embryos. **j** A bar graph of phosphorylated Smad1/5/8 staining level in *gli3^{+/+}*, *gli3^{4ins/14ins}* and *gli2b^{17ins/17ins}* embryos. The fluorescence intensity in the cleithrum was quantified and standardized by the area size in the cleithrum (“Method”). All raw data points were plotted. Raw data are in Supplementary Table 9. The data were analyzed and compared among samples by two-tailed student’s t-test. * indicates $p < 0.05$. p -value between *gli3^{+/+}* and *gli3^{4ins/14ins}* is 0.049 and between *gli3^{+/+}* (WT) and *gli3^{4ins/14ins}* is 0.025. While *gli3^{4ins/14ins}* and *gli2b^{17ins/17ins}; gli3^{4ins/14ins}* embryos exhibit statistically significant reduction of the Psmad1/5/8 signal from wildtype embryos, *gli3^{4ins/14ins}* and *gli2b^{17ins/17ins}; gli3^{4ins/14ins}* embryos do not show statistically significant change ($p = 0.28$). The unit of vertical axis is arbitrary unit. $n = 6, 9$, and 5 biologically independent samples for wildtype embryos, *gli3^{4ins/14ins}* and *gli2b^{17ins/17ins}; gli3^{4ins/14ins}* embryos, respectively. Error bars show standard deviations. **k–l** LDN193189-treated pectoral fins stained by HCR with *sp7* and *col2a1a* probes and DAPI staining. *Sp7* expression was diminished by 10 μM of the inhibitor treatment. Arrows indicate *sp7* expression, and arrowheads show its weak or no expression. sc scapula. $n = 23$ for 0 and 10 μM . The scale bar in (e, g) are 50 μm . **g–i, k, l** are the same scale.

results indicate that the Hedgehog-Gli signaling regulates not only the shoulder girdle bone morphology, but also the ratio of intramembranous and endochondral ossification in pectoral girdle development.

Discussion

The phenotype of *gli3* knockout zebrafish is consistent with those described in tetrapod models, suggesting that the gene’s functions are evolutionarily conserved across bony fishes. We have shown that *gli3^{4ins/14ins}* zebrafish exhibited abnormal skeletogenesis in the skull, eye, and shoulder girdle. The dense mineralization of intramembranous skull bones is a coherent phenotype with human diseases, such as Greig cephalopolysyndactyly⁵². Moreover, expansion of the endochondral scapula in *shha* and *gli3* compound knockout zebrafish is consistent with the scapula phenotype in *Gli3* knockout mice⁴¹. These comparable ossification defects in zebrafish and mammals thus suggest that Gli3 functions are evolutionarily conserved in bone formation at least between actinopterygians and tetrapods. Importantly, previous studies indicate that a reduction of Hedgehog signaling severely affects cleithrum, scapula, and coracoid development in zebrafish⁸⁸. Given these results, we propose that conserved Gli3 functions form the actinopterygian fish pectoral girdle, balancing intramembranous and endochondral ossification.

Polydactyly is a pervasive phenotype in *Gli3*-deficient mammals, and even *gli3* knockout medaka show an increase of fin rays and endochondral radials⁷². The fin phenotype of *gli3^{4ins/14ins}* zebrafish, however, differs from the previously published medaka phenotype⁵⁹; *gli3^{4ins/14ins}* zebrafish did not show the increase of fin rays and endochondral radials. The lack of a bone-increase phenotype in the pectoral fin of *gli3^{4ins/14ins}* zebrafish is consistent with results from a different zebrafish *gli3* knockout allele produced in an independent study⁸⁹ and, thus, is a validated phenotype from multiple studies. This phenotypic difference between zebrafish and medaka might reflect diverse functions of the Hh-Gli signaling in formation of exceptionally diverse pectoral fins and girdles in actinopterygian fishes, including various fin ray numbers, possibly due to differential retention of TGD-duplicated Hh-Gli pathways⁹⁰. Alternatively, the short DNA oligo insertion into *gli3* coding sequence by CRISPR/Cas9 might induce genetic compensation that increases similar gene transcription in zebrafish⁹¹. In addition to Gli3, Gli2 functions as both activator and repressor depending on Hedgehog ligand binding to its receptors⁹². Yet, even *gli2b; gli3* double knockout zebrafish did not manifest the increase of fin rays and radials. Gli2a and Gli2b repressor forms may functionally compensate Gli3

repressor function to restrict the number of fin rays and radials along the anterior-posterior axis in zebrafish. The comprehensive elimination of all *gli2* and *gli3* family genes (i.e., *gli2a*, *gli2b*, and *gli3*) would likely provide “polydactyly” phenotype in zebrafish although the elimination of all Gli2 and Gli3 activator and repressor forms might not provide a conspicuous phenotype, as both activator and repressor forms are critical for distinct domains of paired appendage development in mice⁹². These potential functional compensations among Gli proteins might explain the absence of statistically significant differences of osteoblast and chondrocyte numbers in the pectoral girdle between *gli3* and *gli2b; gli3* knockout embryos.

The morphological transformation of the vertebrate pectoral girdle during the water-to-land transition has been extensively described^{87,93}, yet the underlying ontogenetic changes remain uninvestigated. In the last few decades, zebrafish have emerged as a compelling model to dissect the genetic and molecular pathways underlying diverse arrays of skeletal phenotypes because zebrafish are amenable to various genetic manipulations, live imaging, and produce ample fertilized eggs for embryological experimental studies. Leveraging these zebrafish strengths, our current study illuminates the developmental mechanisms underlying the pectoral girdle evolution, which have been long-debated⁹⁴. Despite the fact that the crown teleost ancestor underwent the TGD that led sub- and neo-functionalization of many gene duplicates^{60,95}, our *Gli3* knockout zebrafish show the evolutionarily conserved the pectoral girdle phenotype. Distinct from sarcopterygians, teleosts mostly use perichondral ossification during development, including pectoral fin and girdle formation^{31,96,97}. Additionally, in teleost fishes, the scapulocoracoid is divided into two distinct elements, the scapula and coracoid. Despite these genomic, ontogenetic, and anatomical specializations, zebrafish Gli3 functions in developing bones, including the scapula, are substantially conserved with extant mammals. Moreover, we identified *acrv11* expression in spotted gar and skate embryonic fin and girdle structures, in which the scapula and coracoid are unified in a single bone, further supporting the evolutionary conservation of Gli3 signaling in ancestral jawed vertebrate pectoral girdle development. Thus, our present study with basal and derived actinopterygians and chondrichthyans provides the first genetic and ontogenetic insights into the pectoral girdle transformation from water to land.

While zebrafish is a compelling model organism to illuminate the molecular mechanisms of skeletal development and evolution, they represent a miniaturized teleost species. Miniaturization causes structural reduction, simplification, and novelty⁹⁸. Haemal arches, for

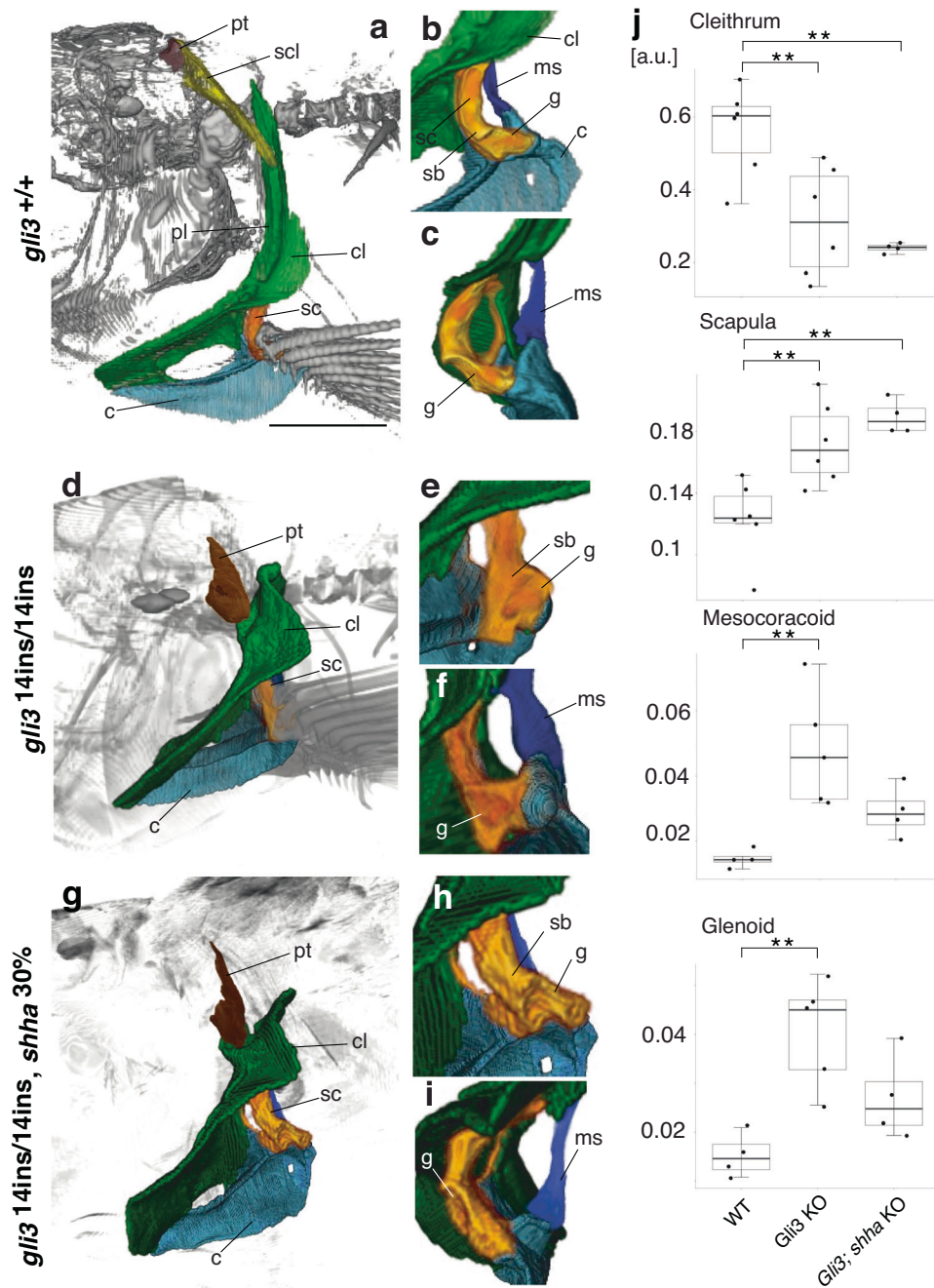


Fig. 4 | Adult pectoral girdle phenotype in Hh-gli signaling knockout fish.

a–c, d–f, g–i Volumetric renderings of the skeleton, which was segmented manually from μ CT scans of three-months old adult fish. **a–c** wildtype, **d–f** *gli3*^{14ins/14ins}, **g–i** *gli3*^{14ins/14ins}; *shha*^{30%KO} fish. **a, d, g** the whole-body 3D reconstruction, (**b, c, e, f, h, i**) the enlarged images of the scapulocoracoid and mesocoracoid (**b, e, h**); lateral view, (**c, f, i**); posterior view. In contrast to the thin and long dorsal cleithrum with the postbranchial lamina in *gli3*^{+/+} fish (**a**), the dorsal cleithrum was reduced in either the left or right side of *gli3*^{14ins/14ins} fish ($n = 28/159$) (**d**) and both sides of *gli3*^{14ins/14ins}; *shha*^{30%KO} fish (3/3) (**g**). In the scapula of *gli3*^{+/+} fish, the glenoid is anteroposteriorly wide and flat (**b, c**), but it is concave and posterolaterally opened, and delineates the proximal surface of basal radials of the pectoral fin in *gli3*^{14ins/14ins} and *gli3*^{14ins/14ins}; *shha*^{30%KO} fish (**e, f, h, i**) ($n = 5/6$ for each genotype). The supraglenoid buttress is more developed in *gli3*^{14ins/14ins} and *gli3*^{14ins/14ins}; *shha*^{30%KO} fish compared to wildtype fish (**b, e, h**). **j** Quantitative analysis of the cleithrum height, scapula width, mesocoracoid width, and glenoid depth. The length and width of each bone were measured and standardized by the dorsoventral length of the skull

(see Methods). The unit is arbitrary unit [a.u.]. All raw measurements are summarized in Supplementary Data 3. While the cleithrum is dorsoventrally shorter in the severely affected pectoral girdles of *gli3*^{14ins/14ins} and *gli3*^{14ins/14ins}; *shha*^{30%KO} fish than those of *gli3*^{+/+} fish, the scapula and mesocoracoid are larger in *gli3*^{14ins/14ins} and *gli3*^{14ins/14ins}; *shha*^{30%KO} fish. The glenoid is more concave in *gli3*^{14ins/14ins} and *gli3*^{14ins/14ins}; *shha*^{30%KO} fish than wildtype fish. ANNOVA test and following Tukey-Kramer Post Hoc test were conducted to detect statistically significant differences of bone size among wildtype and knockout fish. **: absolute mean value > Q critical value in Tukey-Kramer Post Hoc Test. 5.07 and 5.83 > 3.73 in the cleithrum, 5.10 and 6.16 > 3.73 in the scapula, and 6.07 > 3.88 in the mesocoracoid, and 6.05 > 3.88 in the glenoid). Maximum, minimum, median, and average values are shown in the box and whisker plots. Two or three biologically independent fish samples were analyzed in each genotype. Both left and right pectoral girdle measurements are plotted. See all replicates and measurements in Supplementary Data 3. c coracoid, cl cleithrum, g glenoid, ms mesocoracoid, pl postbranchial lamina, sb supraglenoid buttress, and scl supracleithrum. The scale bar indicates 2.5 mm.

example, develop via intramembranous ossification in many small teleost fishes, including zebrafish, but via endochondral ossification in larger teleosts⁹⁹. The coracoid and scapula of *Priocharax ariel*, one of the miniaturized teleost fishes in South America, are not ossified even in adult fish in contrast to full ossification of the cleithrum³⁶. Thus, a caveat of using miniaturized teleost fish for understanding of the pectoral girdle evolution is potential changes in ossification patterns.

During the evolution of the miniaturized body, many endochondral bones in zebrafish shifted from endochondral to perichondral ossification, including the pectoral girdle. The zebrafish scapulocoracoid, the primordium of the scapula and coracoid, is a thin cartilage plate during early development⁸⁴. The coracoid ossification initiates at the dorsal edge of the anterior extension of the scapulocoracoid and spreads to the posterior side via perichondral ossification¹⁰⁰. The different ossification modes of endochondral bones between miniaturized teleosts and stem-tetrapods may hamper us from a direct comparison of pectoral girdle developmental mechanisms. In this study, we hypothesize that the final size and morphology of the scapula and coracoid simply reflect those of cartilage primordium common for perichondral and endochondral ossification. Accordingly, we discuss the molecular and ontogenetic mechanisms underlying changes in the ratio of endochondral and intramembranous bones during the water-to-land transition using zebrafish pectoral girdle as a proxy. However, one may argue that the final size and morphology of the scapula and coracoid might have been modified during the shift from endochondral to perichondral ossification, irrespective of cartilage primordium morphology. Despite such differences in ossification modes between miniaturized teleosts and stem-tetrapods, the molecular mechanisms that induce chondrocyte and osteoblast differentiation are tightly conserved¹⁰¹. The exceptional conservation of ossification genes could justify an evolutionary prevalence of the Gli3 signaling pathway that determines the balance of endochondral and intramembranous ossification. The pectoral girdle evolutionary mechanisms would be further scrutinized by studies with non-miniaturized actinopterygians such as spotted gar, an emerging model without a 3rd round of whole genome duplication and body miniaturization⁹⁵.

The evolutionary trajectory of the intricate shoulder girdle development at the origin of stem-tetrapods has been uncharacterized. By taking advantage of the ontogenetic and genetic accessibility of zebrafish, we discovered that *gli3*-positive mesodermal cells give rise to both intramembranous and endochondral bones in the pectoral girdle (Fig. 5). Our results reveal that modulations in Hh-Gli signaling are plausible evolutionary mechanisms to assemble the tetrapodmorph pectoral girdle through mesodermal cell fate alternations, which have been also reported in the evolution of digits from fin rays^{11,12}. Thus, changes in the fate of mesodermal cells appear to have occurred repeatedly in appendages across the fish-to-tetrapod transition and represent a major path for the evolutionary origin of novel traits.

The dorsoventrally short cleithrum, the loss of the supracleithrum, the posterolaterally oriented concave glenoid, and the robust mesocoracoid in *gli3* single and *gli3:shh* compound knockout zebrafish conform to the shared features of the pectoral girdle bones in Devonian-era stem-tetrapods, such as *Tiktaalik*, *Acanthostega*, and *Ichthyostega*^{6–8} (Fig. 5). Moreover, the concave and posterolaterally-opened glenoid in *gli3*^{314ins/14ins} fish is similar to a prominent feature of the stem-tetrapods. These morphological features permit the rotation, flexion, extension, protraction, and retraction of the humerus⁵. The current work suggests that the Gli3-Acvr1l pathway and their functions in the pectoral girdle formation are evolutionarily conserved at least from basal to derived actinopterygian fishes. Genetic alterations in Hh-Gli or associated signaling pathways, such as the evolutionary reduction and eventual loss of tetrapod *Acvr1l* orthologs, might have

released a deeply embedded developmental program to generate tetrapod morph pectoral girdle phenotypes in bony vertebrates.

Methods

Animal maintenance

All fish work was conducted according to standard protocols approved by the animal committees of Rutgers University (protocol number 201702646) and Michigan State University (PROTO202200367). Skate embryos (*Leucoraja erinacea*) were purchased from Marine Biological Laboratory (Woods Hole, MA), fixed by 4% PFA, and kept in methanol at −20 °C for whole-mount in situ hybridization.

Evolutionary comparisons of *CNE14*

The evolutionary conservation of *gli3* *CNE14* sequence was conducted in mVISTA¹⁰². For this sequence comparison, the following genome regions were downloaded from Ensembl and compared in mVISTA: human: GRCh38:7:41954886:42270163, mouse: GRCm39:13:15632485:15909946, tropical clawed frog: UCB_X-tro_10.0:6:57560778:57692896, elephant shark: *Callorhynchus milii*-6_1_3_K1635914_1_1211641_1411175, spotted gar: LepOcu1_LG9_37116819_37285109, and zebrafish: GRCz11:24:11522406:11827369.

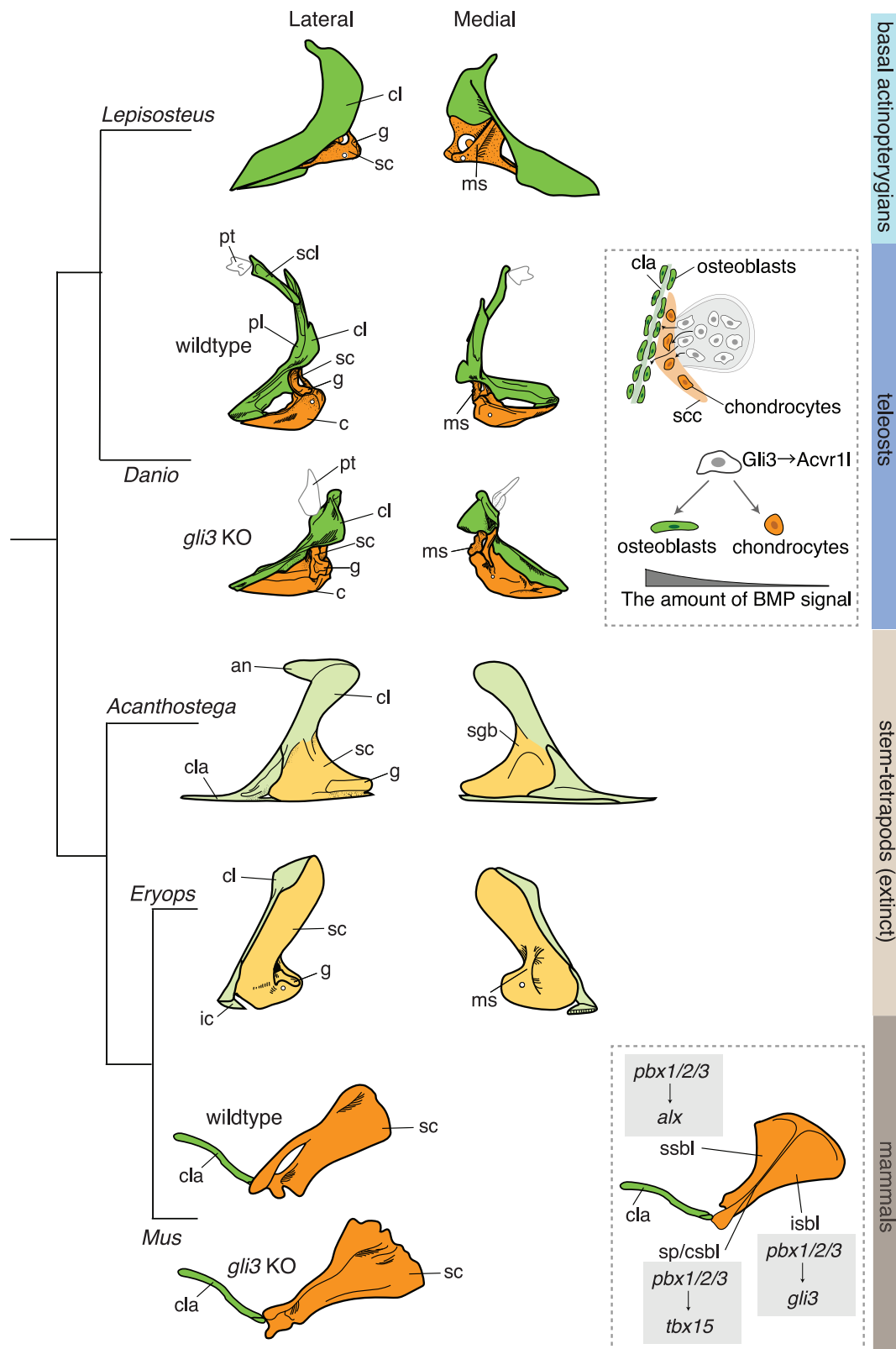
Establishment of *CNE14:egfp* transgenic fish

The region of the zebrafish and elephant shark genome homologous to human *CNE14*²⁶ was amplified by PCR and subcloned pCRTM8/GW/TOPO[®] (Invitrogen) (the primer sequences are in Supplementary Table 1). The cloned *CNE14* fragment was transferred into pXIG-cfos-EGFP vector by GatewayTM LR ClonaseTM II (Invitrogen)⁴⁶. Each *CNE14* / pXIG-cfos-EGFP vector was injected into over 250 one-cell stage zebrafish eggs with Tol2 mRNA as previously described⁴⁷. EGFP fluorescence was observed at 48 hpf under a fluorescence stereomicroscope. For elephant shark *CNE14*, F0 embryos with EGFP expression were raised for three months, and the EGFP expression pattern was confirmed in F1 embryos obtained from outcrossing the F0 to wildtype fish under a stereotypic fluorescent microscope. The embryos with EGFP expression in the pectoral fin were reared to adult stage and further crossed to wildtype fish to establish stable transgenic embryos, which were used for immunofluorescence, HCR in situ hybridization, and live fluorescent imaging.

Whole mount in situ hybridization

The 3'UTR or coding sequence of the zebrafish, skate, and spotted gar genes were amplified from zebrafish (48hpf), skate (stage 31), and spotted gar (stage 28) cDNA by PCR and cloned into pCRTMII-TOPO[®] vector (Invitrogen) (PCR primer sequences are in Supplementary Table 1). The RNA probes were synthesized from the vectors by T7 or SP6 RNA polymerase for zebrafish and skate and from vector insert PCR amplicate for gar.

Chromogenic in situ hybridization for *acvr1l* in zebrafish and skate embryos was performed as previously described⁴⁸. The spotted gar ISH method is based on Thisse & Thisse 2008¹⁰³. In situ hybridization chain reaction (HCR) was performed as previously described⁴⁹ using complementary probes to zebrafish *sp7*, *col2a1a*, *egfp*, *gli3*, which were all synthesized by Molecular Instruments (CA). To observe the HCR results at the single cell resolution, the pectoral fin and girdle complex were manually dissected out from the body with tweezers, mounted on slide glasses, and scanned by a confocal microscope (Zeiss LSM510 META). The number of chondrocytes in the scapulocoracoid (*col2a1a*+) and osteoblasts surrounding the cleithrum at the level of the scapulocoracoid (*sp7*+) were manually counted and statistically compared among different genotypes or embryos treated by different concentrations of the inhibitor by a Student's t-test. For HCR of *sp7*, *col2a1a* and *egfp*, *n* = 23 (Fig. 1e, f). For the staining of *sp7* and *col2a1a* in Fig. 2d–f, all raw data and replicates are shown in Supplementary Table 5.



For fluorescence in situ hybridization of *gli3* mRNA, we followed the protocol previously published in Lauter et al.¹⁰⁴. Briefly, embryos were fixed at 48 hpf by 4% PFA. Next day, following DEPC-PBST (phosphate buffered saline, 0.1% Tween-20, pH 7.3) rinse, the embryos were treated by 2% hydrogen peroxide in methanol for 20 min. After rehydration, embryos were subjected to the previously published whole mount

in situ hybridization protocol⁴⁸. For fluorescent color development, two solutions were prepared: 500 µg/ml Fast Blue (Sigma F3378) or 500 µg/ml NAMP (Sigma N5000) in 0.1M Tris-HCl pH 8.2, containing 50 mM MgCl₂, 100 mM NaCl, and 0.1% Tween-20 were prepared. Before color development, we mixed these two solutions at 1:1 ratio and soaked embryos in the mixed solution until the color developed.

Fig. 5 | Pectoral girdle evolution from fish to tetrapods and Gli3 function in their development. From fish to tetrapods, endochondral bones (scapula and coracoid) expanded at the expense of the intramembranous bones (anocleithrum, cleithrum, and clavicles). In *gli3*^{4ins/14ins} zebrafish, the cleithrum becomes dorso-ventrally short, reminiscent of the pectoral girdles of early tetrapods, such as *Acanthostega*, which were evolving to live on land. *Gli3*-positive cells migrate into the cleithrum and scapulocoracoid, and *Gli3* regulates BMP signaling via *acvr11* expression. In crown-group tetrapods, including mice and chickens, the prospective pectoral girdle cells reside in the proximal region of forelimb buds. *Pbx1/2/3* family genes regulate the expression of *alx*, *tbx15*, and *gli3* in the superior scapula blade (ssbl), inferior scapula blade (isbl), and spine/central scapula blade (sp/

csbl)^{41,119}. The cellular origins of the shoulder girdle bones, shown by light green and orange in *Acanthostega* and *Eryops* are estimations from histological characters, an anocleithrum, c coracoid, cla clavicle, cl cleithrum, g glenoid, ic interclavicle, ms mesocoracoid arch, pl postbranchial lamina, sc scapula, sec scapulocoracoid, scl supracleithrum, sgb supraglenoid buttress. The pectoral girdle of *Mus* was reproduced from the previous study with permission (ref. 41). *Acanthostega* shoulder girdle was reproduced from the previously published article (ref. 7). *Lepisosteus* and *Eryops* were reproduced from previous studies with permission (ref. 87 Copyright © 1924 Wiley-Liss, Inc.). Photos of the pectoral girdle of an adult *Lepisosteus oculatus* are in Supplementary Fig. 16.

Live fluorescence cell imaging

CNE14:egfp transgenic fish were crossed to *sp7:mCherry* fish or *col2a1aBAC:mCherry* fish, and fertilized eggs were collected. Embryos with EGFP expression in the pectoral fin primordium were selected under a fluorescent stereotyped microscope at 31 hpf and embedded in 1% low-melt agarose gel in a glass-bottom 3.5 cm dish⁵⁰. The gel covering the anterior half of embryos was removed to allow normal growth of the embryos. E3 medium including tricaine at 0.003% was added to the dishes, and the dishes were kept inside an incubator chamber at 28 °C by a confocal microscope (Zeiss LSM510) from 32 to 74 hpf. Z-stack images (3 μm z-interval, -30–40 slices for each embryo) were obtained at 30 minutes time intervals. The time lapse data were analyzed with Imaris (version 10.1) to manually track EGFP-positive cell movement and contribution to the cleithrum and scapulocoracoid. The replicate number is three for each transgenic fish imaging.

Establishment of *gli3*, *gli2b:gli3*, and *gli3:shha* compound knockout fish

Gli3 single knockout fish with frameshift mutations in exon5 and exon14 were generated by injection of gRNAs complementary to target sites and *Cas9* mRNA into wildtype (*AB) fertilized eggs as previously reported^{12,105}. The detailed information of gRNAs and identified frameshift mutations are summarized in Supplementary Fig. 1. Briefly, gRNA and *Cas9* mRNA were injected into zebrafish one-cell stage eggs, and the injected eggs were reared to adult fish, which were subjected to T7 assay and sequencing to determine genetic mutations at the target loci. The fish with frame-shift mutations (F0) were out-crossed to wildtype fish to obtain heterozygous knockout fish (F1). To avoid any off-target effects of CRISPR/Cas9 gene deletions on the phenotypic analysis, we repeated outcrossing the heterozygous knockout fish to wildtype fish (*AB) and raising offspring twice, obtaining F4 fish for the analysis conducted in the paper. Then, *gli3 ex5*^{14ins/+} fish (F4) were crossed with each other and *gli3 ex5*^{14ins/14ins} fish were established. The survival rate of *gli3 ex5*^{14ins/14ins} zebrafish is not significantly different from that of wildtype fish and the ratio of *gli3*^{+/+}, *gli3 ex5*^{14ins/+} and *gli3 ex5*^{14ins/14ins} follow Mendelian inheritance ratio. To obtain *gli2/gli2b* compound knockout fish, gRNA complementary to a target site in *gli2b* exon1 and *Cas9* mRNA was injected into one-cell stage *gli3 ex5*^{14ins/14ins} fertilized eggs. The injected eggs were reared to an adult stage and subjected to a T7 assay and sequencing to identify frameshift mutations. The fish with frameshift mutations were outcrossed to *gli3 ex5*^{14ins/14ins} fish and the collected eggs were raised for three months and genotyped for *gli2b*. Obtained *gli2b*^{7ins/+}; *gli3 ex5*^{14ins/14ins} fish were crossed with each other and embryos were subjected to HCR in situ hybridization.

To obtain *gli3/shha* compound knockout fish, gRNA complementary to *shha* and *Cas9* mRNA were injected into *gli3 ex5*^{14ins/14ins} fertilized eggs. The tail fins of 3 month old adult fish were cut and subjected to a T7 assay for the *shha* gene. The tail lysis of the mutant fish was further subjected to deep sequencing of *shha* target loci to determine frameshift mutation ratio among all mutations (Supplementary Table 1).

All gRNA sequence and genotyping primers are summarized in Supplementary Table 1. The frameshift mutations in all mutant fish are in Supplementary Fig. 1.

Genotyping of *gli3* and *gli2b* knockout fish

Adult or embryonic tails were excised and lysed as previously described¹². Using these tail lysis solutions as PCR templates, the *gli3* and *gli2* loci were amplified by PCR. The PCR primers used for PCR amplification are summarized in Supplementary Table 1. For *gli3*, a 14 bp difference between wildtype and mutant fish was confirmed on 3% agarose gels. BSAJ1 was added to *gli2b* PCR products and the treated PCR products were confirmed on 1% agarose gel (wildtype; 232 bp, *gli2b*^{17ins}; 130 + 123 bp).

Live fluorescence imaging of *sp7* expression in the cleithrum

The whole body EGFP expression patterns of *sp7:egfp*; *gli3*^{+/+}, *sp7:egfp*; *gli3*^{14ins/14ins}, *sp7:egfp*; *gli2b*^{17ins/17ins}; *gli3*^{14ins/14ins} embryos were photographed at 72 hpf under Leica M205. The representative images are shown in Supplementary Fig. 8. *n* = 8 for each genotype.

Chemical inhibitor treatment of zebrafish embryos

Zebrafish embryos were cultured in 40 ml of E3 medium (5 mM NaCl, 0.17 mM KCl, 0.33 mM CaCl₂, 0.33 mM MgSO₄) containing Smoothed inhibitor (BMS-833923, Selleckchem) or Activin receptor type 1 inhibitor (LDN-193189, TOCRIS) in 10 cm plastic dishes from 32 hpf to 72 hpf. The concentration of BMS-833923 was 5 μM, and of LDN-193189 was 10 μM. At 72 hpf, these inhibitor-treated embryos were fixed by 4% PFA and subjected to immunofluorescence staining or HCR. All raw data, cell count results, and replicates are summarized in Supplementary Table 5.

FACS sorting of EGFP-positive cells from *CNE14:egfp* fish

Approximately 100,000 EGFP-positive cells were collected from *CNE14:egfp*; *gli3*^{+/+} and *gli3*^{14ins/14ins} fish by FACS as previously described⁵¹. Briefly, *CNE14:egfp*; *gli3*^{+/+} or *gli3*^{14ins/14ins} fish were crossed to wildtype fish or *gli3*^{14ins/14ins} fish, respectively, and fertilized eggs were collected. The eggs were raised to 55 hpf at 27.5 °C. Approximately 200 embryos from each genotype were separately dissociated into single cells. The yolk was removed by de-yolk buffer¹⁰⁶ (55 mM NaCl, 1.8 mM KCl, 1.25 mM NaHCO₃), and embryos were rinsed by PBS. Then, embryos were dissociated into single cells by 0.25% trypsin-EDTA and 4 mg/ml Collagenase with mechanical stress of pipetting at 30 °C. Trypsin was inactivated by adding DMEM-10%FBS medium, and dissociated cells were collected by centrifugation. The cells were resuspended in DMEM-10%FBS and strained by a 40 μm filter (Falcon). Purified single cell suspensions were subject to FACS at Rutgers Flow Cytometry Core Facility (<http://rwjmsl.rwjms.rutgers.edu/flow/>).

RNA-sequencing

Total RNA was immediately extracted from 100,000 EGFP-positive cells isolated by FACS using Trizol (Invitrogen). Briefly, the cell suspension was mixed with 1 ml of Trizol by vigorous vortexing and kept for 5 min at room temperature. The mixed solution was

centrifuged, and the supernatant was transferred to a new tube. Chloroform (0.2 ml) was added, vigorously vortexed, and centrifuged for 15 min. The supernatant was mixed with 0.5 ml of isopropanol, kept for 10 min at room temperature, and then centrifuged for 15 minutes. The precipitated RNA was washed by 70% ethanol and reconstituted in 30 μ L water. The RNA samples were submitted to Novogene (CA, USA), converted to sequencing library, and sequenced.

ATAC-sequencing

ATAC-sequencing was performed according to the previously described protocol⁵². Approximately 100,000 EGFP cells isolated by FACS were rinsed in PBS and resuspended in lysis buffer (10 mM Tris-HCl, pH 7.4, 10 mM NaCl, 3 mM MgCl₂, 0.1% NP40). Cells were kept on ice for 10 minutes and then centrifuged at 500 g for 10 min at 4 °C. The pellets were resuspended in the reaction buffer (25 μ L TD Buffer (Illumina Cat #FC-121-1030), 2.5 μ L Tn5 Transposase (Illumina Cat #FC-121-1030), and 22.5 μ L H₂O). Cells were kept at 37 °C for 30 minutes and then purified by Qiagen MinElute Kit. The DNA was eluted with 10 μ L of Elution buffer. Open chromatin regions flanked by the adapter sequence were amplified with 14 cycles by the thermal cycler with Illumina/Nextera i5 common adapter and i7 index adapters. The amplified sequencing library was submitted to BGI and sequencing was performed by the paired-end, 100 bp reading.

Sequencing data analysis

The quality of RNA-sequencing data (FASTQ format) was analyzed by FastQC¹⁰⁷. Then, after the adapter sequencing primers were removed by Trimmomatic¹⁰⁸, the data were mapped on zebrafish genome (GRCz10) by HISAT2¹⁰⁹. The read numbers for genes were counted by HTSeq¹¹⁰, and differentially expressed genes were determined by EdgeR¹¹¹ in R (R 4.2.2). Following differential gene expression analysis, a heatmap and volcano plot were generated using the “Heatplus” and “EnhancedVolcano” packages in R, respectively.

ATAC-Seq analysis was carried out through multiple programs in Linux. FastQC was used to get a raw quality read of the data, then low-quality reads and sequencing adapters were removed by Trimmomatic. HISAT2 mapped these reads on the zebrafish genome (GRCz10). PCR duplicates were removed with Picard (<http://broadinstitute.github.io/picard/>), and MACS2 was used to call peaks of open chromatin regions¹¹². HOMER was used to identify Gli3 binding regions in ATAC-seq peaks and provide their gene name/specific chromosomal location¹¹³.

Phylogeny and syntenic analysis

Activin receptor type 1 gene family members across vertebrate lineages were identified via Blast searches in the Ensembl and NCBI genome databases using sequences from lineage-representative species as queries (e.g., spotted gar for ray-finned fishes). Survey results and accession numbers are listed in Supplementary Table 8. Protein sequences were aligned using MAFFT v7.490¹¹⁴. A Maximum Likelihood phylogeny from lineage-representative species was generated with PhyML v3.3.20180621¹¹⁵ (LG model, 100 bootstrap replicates). Syntenic conservation around activin receptor genes was analyzed with the Genomic Browser version 04.02¹¹⁶.

CT scanning and quantitative analysis

To identify adult zebrafish bone phenotypes, three-month old fish (wildtype, *gli3*, and *gli3:Shh* compound mutant lines, the total body length spanning from 2.7 to 3.3 cm) were fixed with 10% formalin overnight, stained by 0.5% phosphomolybdic acid for a week followed by water rinse several times, and micro-CT scanned at The University of Chicago (PaleoCT: <https://luolab.uchicago.edu/paleoct/>). Voxel size varied from 5.18 to 8.26 μ m depending on the distance between the specimens and the beam directional tube. The pectoral girdle bones

were manually segmented, reconstructed into 3D, and visualized using Amira 2019.4 (Fisher).

To quantify the size and shape of the pectoral girdle, twenty landmarks were used (see Supplementary Fig. 13). The dorsal, anterior, and posterior extremities of the cleithrum were defined as A, G, and C, respectively. The attachment position of the scapula to the cleithrum was defined as D. The length between the dorsal and posteroventral extremities (A-D) was defined as the cleithrum height. The anterior-posterior cleithrum length was measured by extending the horizontal line anteriorly from C (B-C). The anterior-posterior coracoid length was determined by the anterior and posterior extremities of the coracoid (H-I). Following, a perpendicular line to the H-I line was drawn to maximize its length (J-K) as a coracoid height. The scapula height was determined by the dorsal and ventral extremities of the scapula (D-L). To measure the scapula width, a perpendicular line to the D-L was drawn at its center position (E-F). From the posterior view, a straight line was drawn between the dorsal and ventral edges of the glenoid fossa (M and N). Then, a perpendicular line from the M-N line to the bottom of the glenoid fossa was drawn to maximize its length (O-P; the glenoid fossa depth). The mesocoracoid height was determined by the dorsal and ventral extremities of the mesocoracoid from the posterior view (R-Q). An orthogonal line to the R-Q line at its center position was drawn as the mesocoracoid width (S-T). Each length was measured in Amira and standardized by the length of the skull height. The raw measurements are in Supplementary Data 3. The volumes of the cleithrum, coracoid, and scapula of wildtype, *gli3*^{4ins/14ins}, *gli3*^{4ins/14ins}, *shha*^{30x} fish were digitally measured in Amira and summarized in Supplementary Data 4. Replicates of CT analysis represent 3, 5, and 2 individuals for wildtype, *gli3*, and *gli3:shh* compound mutant fishes, respectively. The telencephalon length along the anterior-posterior axis was measured and standardized by the length from the most anterior tip of the head to the first vertebra in wildtype and *gli3*^{4ins/14ins} fish (three replicates each).

Immunofluorescence staining and signal quantification

Immunofluorescence staining of EGFP and phosphorylated Smad 1/5/8 was conducted following the previously described protocol⁵³. After EGFP or phosphorylated Smad 1/5/8 was stained, the plasma membrane and nuclei were stained by CellMask (1/1000 dilution, Invitrogen) and DAPI (1/4000 dilution) in PBS containing 0.1% TritonX-100. EGFP antibody (Abcam #ab290) and phosphorylated Smad 1/5/8 antibody (Cell Signaling #13820) were used at 1/1000 and 1/100 dilution, respectively. For the detection of the first antibody, anti-mouse Alexa 488 (Invitrogen #A21206) was used at 1/1000 dilution. The stained pectoral fin and girdles were photographed by a confocal microscope (LSM510). After photographing of the staining samples, the signal intensity of phosphorylated Smad 1/5/8 was quantified using ImageJ. The cleithrum region is manually identified as Region Of Interest and the signal intensity/area size was measured by ImageJ function.

Gross observation and whole-mount bone and cartilage staining

Gross morphology observation of adult *gli3*^{4ins/14ins}, *gli2b*^{17ins/17ins}, *gli2b*^{17ins/17ins}, *gli3*^{4ins/14ins}, and *gli3*^{4ins/14ins}; *shha*^{30x} fish were conducted under Leica M205 stereomicroscopy. The replicate number of each genotype is 159, 21, 9, and 3, respectively. The total body length of these fish were between 2.8 to 3.4 cm. The fish used for gross observation was subjected to whole mount skeletal staining. Whole-mount skeletal staining of adult zebrafish with Alizarin red and Alcian blue was conducted as follows. The specimens were anesthetized and fixed by 10% neutral-buffered formalin at room temperature overnight. After rinsing with water, their entrails were manually removed, and the remaining body was immersed in 70% ethanol. The solution was replaced by 70% ethanol / 30% acetic acid with 0.02% of Alcian Blue 8GX (Sigma-Aldrich A5268), and the samples were incubated at room temperature overnight. The specimens were rinsed by a series of

ethanol/water mix solutions (75%, 50%, 25%, and 0% ethanol) for an hour each. Then they were immersed in 30% saturated sodium borate for an hour. The specimens were treated by 0.25% trypsin for five hours and washed by 1% potassium hydroxide solution twice. The solution was replaced by 0.005% Alizarin red S (Sigma-Aldrich A5533) /1% potassium hydroxide, and incubated at room temperature overnight. The stained specimens were bleached in 25% glycerol/75% 0.1% potassium hydroxide/0.15% hyrdoxidase solution for five hours. The specimens were soaked through a series of 0.1% potassium hydroxide/glycerol solutions (75%, 50%, 25%, and 0% potassium hydroxide) and preserved in 100% glycerol solution. The replicate number of adult *gli3*^{4ins/14ins}, *gli2b*^{17ins/17ins}, *gli2b*^{17ins/17ins}, *gli3*^{4ins/14ins}, and *gli3*^{4ins/14ins}, *shha*^{30%} fish used for skeletal staining were 7, 8, 5, and 3, respectively.

For juveniles at 13–30 dpf, to avoid acid demineralization of bones, we conducted acid-free skeletal staining as previously published¹¹⁷. Briefly, we prepared two stock solutions. One is 0.02% alcian blue, 60 mM (13 dpf) or 120 mM (30 dpf) MgCl₂, and 70% ethanol, and the other is 0.5% alizarin red S powder dissolved in water. We mixed these Alcian blue and alizarine red solutions at 100:1 ratio. Then, juveniles fixed by 4% PFA for two hours at room temperature were stained in this solution overnight. Next day, the juveniles were bleached in 1.5% H₂O₂ and 1% KOH solution and moved to 50 % glycerol solution. The juvenile sizes for gross observation and skeletal staining are shown in the Supplementary Fig. legends. Replicate number for each genotype at each stage varies from 2 to 8. The number of obtained juveniles is summarized in Supplementary Table 2.

A quantification for the dorsal shift of the pectoral girdle

The dorsoventral body height at the pectoral position was measured with wildtype and *gli3*^{4ins/14ins} fish. The vertical length between the proximal end of the first fin ray and the ventral edge of the body was also measured and standardized by the dorsoventral body height.

Skeletal preparation of the spotted gar pectoral girdle bone

An adult, wild-caught spotted gar (*Lepisosteus oculatus*, total length was 61 cm) was euthanized with overdose of MS-222 (Tricaine) and then boiled for 10 min in water. The pectoral girdle complex was dissected out, and muscles and connective tissues were manually removed by tweezers. The cleaned pectoral girdle bones were photographed by Canon EOS R6 camera.

Reporting summary

Further information on research design is available in the Nature Portfolio Reporting Summary linked to this article.

Data availability

Raw sequence and processed BAM files of RNA-seq and ATAC-seq are available at the National Center for Biotechnology Information Sequence Read Archives (NCBI SRA), www.ncbi.nlm.nih.gov/sra (BioProject accession code no PRJNA767802). Source data are provided with this paper.

References

- Clack, J. A. The fish-tetrapod transition: new fossils and interpretations. *Evolut. Educ. Outreach* **2**, 213–223 (2009).
- Hirasawa, T. & Kuratani, S. Evolution of the vertebrate skeleton: morphology, embryology, and development. *Zool. Lett.* **1**, 2 (2015).
- Wood, T. W. P. & Nakamura, T. Problems in fish-to-tetrapod transition: genetic expeditions into old specimens. *Front. Cell Dev. Biol.* **6**, 70–70 (2018).
- Goodrich, E. S. *Studies on the structure & development of vertebrates*. (MacMillan and Co., Limited, 1930).
- Romer, A. S. *The Vertebrate Body*. p. 643 (W. B. Saunders Company, Philadelphia, 1949).
- Shubin, N. H., Daeschler, E. B. & Jenkins, F. A. The pectoral fin of *Tiktaalik roseae* and the origin of the tetrapod limb. *Nature* **440**, 764–771 (2006).
- Coates, M. I. The Devonian tetrapod *Acanthostega gunnari* Jarvik: postcranial anatomy, basal tetrapod interrelationships and patterns of skeletal evolution. *Trans. R. Soc. Edinb. Earth Sci.* **87**, 363–421 (1996).
- Ahlberg, P. E., Clack, J. A. & Blom, H. The axial skeleton of the Devonian tetrapod *Ichthyostega*. *Nature* **437**, 137–140 (2005).
- Daeschler, E. B., Shubin, N. H. & Jenkins, F. A. A Devonian tetrapod-like fish and the evolution of the tetrapod body plan. *Nature* **440**, 757–763 (2006).
- Smith, M. M. & Hall, B. K. Development and evolutionary origins of vertebrate skeletogenic and odontogenic tissues. *Biol. Rev. Camb. Philos. Soc.* **65**, 277–373 (1990).
- Hawkins, M. B., Henke, K. & Harris, M. P. Latent developmental potential to form limb-like skeletal structures in zebrafish. *Cell* **184**, <https://doi.org/10.1016/j.cell.2021.01.003> (2021).
- Nakamura, T., Gehrke, A. R., Lemberg, J., Szymaszek, J. & Shubin, N. H. Digits and fin rays share common developmental histories. *Nature* **8**, 225–228 (2016).
- Shimada, A. et al. Trunk exoskeleton in teleosts is mesodermal in origin. *Nat. Commun.* **4**, 1639–1639 (2013).
- Nagashima, H. et al. Developmental origin of the clavicle, and its implications for the evolution of the neck and the paired appendages in vertebrates. *J. Anat.* **229**, 536–548 (2016).
- McGonnell, I. M., McKay, I. J. & Graham, A. A population of caudally migrating cranial neural crest cells: functional and evolutionary implications. *Dev. Biol.* **236**, 354–363 (2001).
- Chevallier, A. Origines des ceintures scapulaires et pelviennes chez l'embryon d'oiseau. *J. Exp. Morphol. Embryol.* **42**, 275–292 (1997).
- Heude, E. et al. Unique morphogenetic signatures define mammalian neck muscles and associated connective tissues. *Elife* **7**, <https://doi.org/10.7554/eLife.40179> (2018).
- Adachi, N., Bilio, M., Baldini, A. & Kelly, R. G. Cardiopharyngeal mesoderm origins of musculoskeletal and connective tissues in the mammalian pharynx. *Development* **147**, <https://doi.org/10.1242/dev.185256> (2020).
- Huang, R., Zhi, Q., Patel, K., Wilting, J. & Christ, B. Dual origin and segmental organisation of the avian scapula. *Development* **127**, 3789–3794 (2000).
- Piekarski, N. & Olsson, L. A somitic contribution to the pectoral girdle in the axolotl revealed by long-term fate mapping. *Evolut. Dev.* **13**, 47–57 (2011).
- Durland, J. L., Sferlazzo, M., Logan, M. & Burke, A. C. Visualizing the lateral somitic frontier in the Prx1Cre transgenic mouse. *J. Anat.* **212**, 590–602 (2008).
- Valasek, P. et al. Somitic origin of the medial border of the mammalian scapula and its homology to the avian scapula blade. *J. Anat.* **216**, 482–488 (2010).
- Shearman, R. M., Tulenko, F. J. & Burke, A. C. 3D reconstructions of quail-chick chimeras provide a new fate map of the avian scapula. *Dev. Biol.* **355**, 1–11 (2011).
- Burke, A. C. The development and evolution of the turtle body plan: inferring intrinsic aspects of the evolutionary process from experimental embryology. *Am. Zool.* **31**, 616–627 (1991).
- Matsuoka, T. et al. Neural crest origins of the neck and shoulder. *Nature* **436**, 347–355 (2005).
- Epperlein, H.-H., Khattak, S., Knapp, D., Tanaka, E. M. & Malashichev, Y. B. Neural crest does not contribute to the neck and shoulder in the axolotl (*Ambystoma mexicanum*). *PLoS one* **7**, e52244–e52244 (2012).
- Kuroda, S., Lalonde, R. L., Mansour, T. A., Mosimann, C. & Nakamura, T. Multiple embryonic sources converge to form the pectoral girdle skeleton in zebrafish. *Nat. Commun.* **15**, 6313 (2024).

28. Chakrabarty, P. et al. Phylogenomic systematics of ostariophysan fishes: ultraconserved elements support the surprising non-monophyly of characiformes. *Syst. Biol.* **66**, 881–895 (2017).
29. Andrews, S. M. & Westoll, T. S. IX.—The postcranial skeleton of *Ensthenopteron foordi* Whiteaves. *Earth Environ. Sci. Trans. R. Soc. Edinb.* **68**, 391–489 (1970).
30. Mansuit, R. et al. Development and growth of the pectoral girdle and fin skeleton in the extant coelacanth *Latimeria chalumnae*. *J. Anat.* **236**, 493–509 (2020).
31. Desvignes, T., Carey, A., Braasch, I., Enright, T. & Postlethwait, J. H. Skeletal development in the heterocercal caudal fin of spotted gar (*lepisosteus oculatus*) and other lepisosteiformes. *Dev. Dyn.* **247**, 724–740 (2018).
32. Hall, B. K. *Evolutionary Developmental Biology, Second edition, Chapter 16*, 255–279. (Springer Netherlands, 1999).
33. Hall, B. K. *Fins into limbs: evolution, development, and transformation, Part 2*, 6, 79–92. (University of Chicago Press, 2007).
34. Witten, P. E. & Villwock, W. Growth requires bone resorption at particular skeletal elements in a teleost fish with acellular bone (*Oreochromis niloticus*, Teleostei: Cichlidae). *J. Appl. Ichthyol.* **13**, 149–158 (1997).
35. Weitzman, S. H. & Fink, W. L. Relationships of the neon tetras, a group of South American freshwater fishes (Teleostei, Characidae), with comments on the phylogeny of New World characiforms. *Bull. Mus. Comp. Zool. Harv. Coll.* **150**, 339–395 (1983).
36. Weitzman, S. H. & Vari, R. P. Two new species and a new genus of miniature characid fishes (Teleostei: Characiformes) from Northern South America. *Proc. Biol. Soc. Wash.* **100**, 640–652 (1987).
37. Roberts, T. R. *Danionella-Translucida*, a new genus and species of cyprinid fish from Burma, one of the smallest living vertebrates. *Environ. Biol. Fishes* **16**, 231–241 (1986).
38. Huysseune, A. *The Laboratory Fish, Handbook of Experimental Animals, Chapter 18—Skeletal System*, 307–317. (Academic Press, 2000).
39. Lleras-Forero, L., Winkler, C. & Schulte-Merker, S. Zebrafish and medaka as models for biomedical research of bone diseases. *Dev. Biol.* **457**, 191–205 (2020).
40. Capellini, T. D. et al. Scapula development is governed by genetic interactions of Pbx1 with its family members and with Emx2 via their cooperative control of Alx1. *Development* **137**, 2559–2569 (2010).
41. Kuijper, S. et al. Genetics of shoulder girdle formation: roles of Tbx15 and aristaless-like genes. *Development* **132**, 1601–1610 (2005).
42. Aubin, J., Lemieux, M., Moreau, J., Lapointe, J. & Jeannotte, L. Cooperation of Hoxa5 and Pax1 genes during formation of the pectoral girdle. *Dev. Biol.* **244**, 96–113 (2002).
43. Timmons, P. M., Wallin, J., Rigby, P. W. & Balling, R. Expression and function of Pax 1 during development of the pectoral girdle. *Development* **120**, 2773–2785 (1994).
44. Rallis, C. et al. Tbx5 is required for forelimb bud formation and continued outgrowth. *Development* **130**, 2741–2751 (2003).
45. Ahn, D.-g., Kourakis, M. J., Rohde, L. A., Silver, L. M. & Ho, R. K. T-box gene *tbx5* is essential for formation of the pectoral limb bud. *Nature* **417**, 754–758 (2002).
46. Heude, É., Shaikho, S. & Ekker, M. The *dlx5a/dlx6a* genes play essential roles in the early development of zebrafish median fin and pectoral structures. *PLoS ONE* **9**, e98505–e98505 (2014).
47. Grandel, H. et al. Retinoic acid signalling in the zebrafish embryo is necessary during pre-segmentation stages to pattern the anterior-posterior axis of the CNS and to induce a pectoral fin bud. *Development* **129**, 2851–2865 (2002).
48. Farmer, D. T., Patel, P., Choi, R., Liu, C. Y. & Crump, J. G. A comprehensive series of *lrx* cluster mutants reveals diverse roles in facial cartilage development. *Development* **148**, dev197244 (2021).
49. Ingham, P. W. & McMahon, A. P. Hedgehog signaling in animal development: paradigms and principles. *Genes Dev.* **15**, 3059–3087 (2001).
50. Hui, C.-c. & Angers, S. Gli proteins in development and disease. *Annu. Rev. Cell Dev. Biol.* **27**, 513–537 (2011).
51. Matissek, S. J. & Elswa, S. F. GLI3: a mediator of genetic diseases, development and cancer. *Cell Commun. Signal.* **18**, 1–20 (2020).
52. Vortkamp, A., Gessler, M. & Grzeschik, K. H. GLI3 zinc-finger gene interrupted by translocations in Greig syndrome families. *Nature* **352**, 539–540 (1991).
53. Biesecker, L. G. in *GeneReviews(R)* (eds M. P. Adam et al.) (1993).
54. Wang, B., Fallon, J. F. & Beachy, P. A. Hedgehog-regulated processing of Gli3 produces an anterior/posterior repressor gradient in the developing vertebrate limb. *Cell* **100**, 423–434 (2000).
55. Litingtung, Y., Dahn, R. D., Li, Y., Fallon, J. F. & Chiang, C. Shh and Gli3 are dispensable for limb skeleton formation but regulate digit number and identity. *Nature* **418**, 979–983 (2002).
56. Riddle, R. D., Johnson, R. L., Laufer, E. & Tabin, C. Sonic hedgehog mediates the polarizing activity of the ZPA. *Cell* **75**, 1401–1416 (1993).
57. Sheth, R. et al. Hox genes regulate digit patterning by controlling the wavelength of a Turing-type mechanism. *Science* **338**, 1476–1480 (2012).
58. Te Welscher, P. et al. Progression of vertebrate limb development through SHH-mediated counteraction of GLI3. *Science* **298**, 827–830 (2002).
59. Letelier, J. et al. The Shh/Gli3 gene regulatory network precedes the origin of paired fins and reveals the deep homology between distal fins and digits. *Proc. Natl. Acad. Sci. USA* **118**, <https://doi.org/10.1073/pnas.2100575118> (2021).
60. Pasquier, J. et al. Evolution of gene expression after whole-genome duplication: new insights from the spotted gar genome. *J. Exp. Zool. B Mol. Dev. Evol.* **328**, 709–721 (2017).
61. Neumann, C. J., Grandel, H., Gaffield, W., Schulte-Merker, S. & Nusslein-Volhard, C. Transient establishment of anteroposterior polarity in the zebrafish pectoral fin bud in the absence of sonic hedgehog activity. *Development* **126**, 4817–4826 (1999).
62. Letelier, J. et al. A conserved Shh cis-regulatory module highlights a common developmental origin of unpaired and paired fins. *Nat. Genet.* **50**, 504–509 (2018).
63. te Welscher, P., Fernandez-Teran, M., Ros, M. A. & Zeller, R. Mutual genetic antagonism involving GLI3 and dHAND prepatterns the vertebrate limb bud mesenchyme prior to SHH signaling. *Genes Dev.* **16**, 421–426 (2002).
64. Buscher, D., Bosse, B., Heymer, J. & Ruther, U. Evidence for genetic control of Sonic hedgehog by Gli3 in mouse limb development. *Mech. Dev.* **62**, 175–182 (1997).
65. Hui, C. C., Slusarski, D., Platt, K. A., Holmgren, R. & Joyner, A. L. Expression of three mouse homologs of the *Drosophila* segment polarity gene *cubitus interruptus*, Gli, Gli-2, and Gli-3, in ectoderm- and mesoderm-derived tissues suggests multiple roles during postimplantation development. *Dev. Biol.* **162**, 402–413 (1994).
66. Venkatesh, B. et al. Elephant shark genome provides unique insights into gnathostome evolution. *Nature* **505**, 174–179 (2014).
67. Nakashima, K. et al. The novel zinc finger-containing transcription factor osterix is required for osteoblast differentiation and bone formation. *Cell* **108**, 17–29 (2002).
68. Spranger, J., Winterpacht, A. & Zabel, B. The type II collagenopathies: a spectrum of chondrodysplasias. *Eur. J. Pediatr.* **153**, 56–65 (1994).
69. Kague, E. et al. Osterix/Sp7 limits cranial bone initiation sites and is required for formation of sutures. *Dev. Biol.* **413**, 160–172 (2016).
70. Askary, A. et al. Iroquois proteins promote skeletal joint formation by maintaining chondrocytes in an immature state. *Dev. Cell* **35**, 358–365 (2015).

71. Naruse, I. et al. Birth defects caused by mutations in human GLI3 and mouse Gli3 genes. *Congenit. Anom.* **50**, 1–7 (2010).
72. Letelier, J. et al. The Shh/Gli3 gene regulatory network precedes the origin of paired fins and reveals the deep homology between distal fins and digits. *Proc Natl. Acad. Sci. USA* **118**, e2100575118 (2021).
73. Tanaka, Y. et al. K. Anterior-posterior constraint on Hedgehog signaling by hh in teleost fin elaboration. *Development* **151**, dev202526 (2024).
74. Almuraikhi, N. et al. Hedgehog signaling inhibition by smoothened antagonist BMS-833923 reduces osteoblast differentiation and ectopic bone formation of human skeletal (mesenchymal) stem cells. *Stem Cells Int.* **2019**, <https://doi.org/10.1155/2019/3435901> (2019).
75. Vokes, S. A., Ji, H., Wong, W. H. & McMahon, A. P. A genome-scale analysis of the cis-regulatory circuitry underlying sonic hedgehog-mediated patterning of the mammalian limb. *Genes Dev.* **22**, 2651–2663 (2008).
76. Mullins, M. C. et al. Genes establishing dorsoventral pattern formation in the zebrafish embryo: the ventral specifying genes. *Development* **123**, 81–93 (1996).
77. ten Dijke, P. et al. Identification of type I receptors for osteogenic protein-1 and bone morphogenetic protein-4. *J. Biol. Chem.* **269**, 16985–16988 (1994).
78. Lavery, K., Swain, P., Falb, D. & Alaoui-Ismaïli, M. H. BMP-2/4 and BMP-6/7 differentially utilize cell surface receptors to induce osteoblastic differentiation of human bone marrow-derived mesenchymal stem cells. *J. Biol. Chem.* **283**, 20948–20958 (2008).
79. Fujii, M. et al. Roles of bone morphogenetic protein type I receptors and Smad proteins in osteoblast and chondroblast differentiation. *Mol. Biol. Cell* **10**, 3801–3813 (1999).
80. Zhang, D. et al. ALK2 functions as a BMP type I receptor and induces Indian hedgehog in chondrocytes during skeletal development. *J. Bone Min. Res.* **18**, 1593–1604 (2003).
81. Franke, M. et al. CTCF knockout in zebrafish induces alterations in regulatory landscapes and developmental gene expression. *Nat. Commun.* **12**, 5415 (2021).
82. Yu, P. B. et al. BMP type I receptor inhibition reduces heterotopic ossification. *Nat. Med.* **14**, 1363–1369 (2008).
83. Grande, L. *An empirical synthetic pattern study of gars (Lepisosteiformes) and closely related species, based mostly on skeletal anatomy: the resurrection of Holosteii*. (American Society of Ichthyologists and Herpetologists (ASIH), 2010).
84. Grandel, H. & Schulte-Merker, S. The development of the paired fins in the zebrafish (*Danio rerio*). *Mech. Dev.* **79**, 99–120 (1998).
85. Lebedev, O. A. & Coates, M. I. The postcranial skeleton of the Devonian tetrapod *Tulerpeton curtum* Lebedev. *Zool. J. Linn. Soc.* **114**, 307–348 (1995).
86. Johanson, Z., Joss, J. M. P. & Wood, D. The scapulocoracoid of the Queensland lungfish *Neoceratodus forsteri* (Dipnoi: Sarcopterygii): morphology, development and evolutionary implications for bony fishes (Osteichthyes). *Zoology* **107**, 93–109 (2004).
87. Romer, A. S. Pectoral limb musculature and shoulder girdler structure in fish and tetrapods. *Anat. Rec.* **27**, 119–143 (1924).
88. Grandel, H., Draper, B. W. & Schulte-Merker, S. Dackel acts in the ectoderm of the zebrafish pectoral fin bud to maintain AER signaling. *Development* **127**, 4169–4178 (2000).
89. Tanaka, M. Alterations in anterior-posterior patterning and its accompanying changes along the proximal-distal axis during the fin-to-limb transition. *genesis* **56**, e23053–e23053 (2018).
90. Furutani-Seiki, M. & Wittbrodt, J. Medaka and zebrafish, an evolutionary twin study. *Mech. Dev.* **121**, 629–637 (2004).
91. El-Brolosy, M. A. et al. Genetic compensation triggered by mutant mRNA degradation. *Nature* **568**, 193–197 (2019).
92. Bowers, M. et al. Limb anterior-posterior polarity integrates activator and repressor functions of GLI2 as well as GLI3. *Dev. Biol.* **370**, 110–124 (2012).
93. Dial, K. P., Shubin, N. & Brainerd, E. L. (eds) *Great transformations in vertebrate evolution*. (University of Chicago Press, Chicago, 2015).
94. Westoll, T. S., Andrews, S. M., Miles, R. S. & Walker, A. D. *Problems in vertebrate evolution: essays presented to Professor T.S. Westoll*. (Linnean Society of London by Academic Press, 1977).
95. Braasch, I. et al. The spotted gar genome illuminates vertebrate evolution and facilitates human-teleost comparisons. *Nat. Genet.* **48**, 427–437 (2016).
96. Hall, B. K. *Fins into limbs: evolution, development, and transformation*. (University of Chicago Press, 2007).
97. Hall, B. K. *Evolutionary developmental biology*. (Springer Science & Business Media, 2012).
98. Hanken, J. & Wake, D. B. Miniaturization of body-size—organismal consequences and evolutionary significance. *Annu. Rev. Ecol. Syst.* **24**, 501–519 (1993).
99. Le Pabic, P., Dranow, D. B., Hoyle, D. J. & Schilling, T. F. Zebrafish endochondral growth zones as they relate to human bone size, shape and disease. *Front Endocrinol. (Lausanne)* **13**, 1060187 (2022).
100. Cubbage, C. C. & Mabee, P. M. Development of the cranium and paired fins in the zebrafish *Danio rerio* (Ostariophysi, Cyprinidae). *J. Morphol.* **229**, 121–160 (1996).
101. Tonelli, F. et al. Zebrafish: a resourceful vertebrate model to investigate skeletal disorders. *Front. Endocrinol.* **11**, 489 (2020).
102. Frazer, K. A., Pachter, L., Poliakov, A., Rubin, E. M. & Dubchak, I. VISTA: computational tools for comparative genomics. *Nucleic Acids Res.* **32**, W273–W279 (2004).
103. Thisse, C. & Thisse, B. High-resolution in situ hybridization to whole-mount zebrafish embryos. *Nat. Protoc.* **3**, 59–69 (2007). 2008 3:1.
104. Lauter, G., Söll, I. & Hauptmann, G. Two-color fluorescent in situ hybridization in the embryonic zebrafish brain using differential detection systems. *BMC Dev. Biol.* **11**, 43 (2011).
105. Nakayama, T. et al. Simple and efficient CRISPR/Cas9-mediated targeted mutagenesis in *Xenopus tropicalis*. *Genes* **51**, 835–843 (2013).
106. McGarvey, A. C. et al. Single-cell-resolved dynamics of chromatin architecture delineate cell and regulatory states in zebrafish embryos. *Cell Genom.* **2**, 100083 (2022).
107. Andrews, S. FastQC: A quality control tool for high throughput sequence data. (2011).
108. Bolger, A. M., Lohse, M. & Usadel, B. Trimmomatic: a flexible trimmer for Illumina sequence data. *Bioinformatics* **30**, 2114–2120 (2014).
109. Goldstein, L. D. et al. Prediction and quantification of splice events from RNA-seq data. *PLoS ONE* **11**, e0156132–e0156132 (2016).
110. Putri, G. H., Anders, S., Pyl, P. T., Pimanda, J. E. & Zanini, F. Analysing high-throughput sequencing data in Python with HTSeq 2.0. *Bioinformatics* **38**, 2943–2945 (2022).
111. Kvam, V. M., Liu, P. & Yaqing, S. A comparison of statistical methods for detecting differentially expressed genes from RNA-seq data. *Am. J. Bot.* **99**, 248–256 (2012).
112. Grytten, I. et al. Graph peak caller: calling chip-seq peaks on graph-based reference genomes. *PLoS Comput. Biol.* **15**, e1006731–e1006731 (2019).
113. Heinz, S. et al. Simple combinations of lineage-determining transcription factors prime cis-regulatory elements required for macrophage and B cell identities. *Mol. Cell* **38**, 576–589 (2010).
114. Katoh, K. & Standley, D. M. MAFFT multiple sequence alignment software version 7: improvements in performance and usability. *Mol. Biol. Evol.* **30**, 772–780 (2013).
115. Guindon, S. et al. New algorithms and methods to estimate maximum-likelihood phylogenies: assessing the performance of PhyML 3.0. *Syst. Biol.* **59**, 307–321 (2010).

116. Parey, E. et al. Genome structures resolve the early diversification of teleost fishes. *Science* **379**, 572–575 (2023).
117. Walker, M. B. & Kimmel, C. B. A two-color acid-free cartilage and bone stain for zebrafish larvae. *Biotech. Histochem.* **82**, 23–28 (2007).
118. Marletaz, F. et al. The little skate genome and the evolutionary emergence of wing-like fins. *Nature* **616**, 495–503 (2023).
119. Young, M., Selleri, L. & Capellini, T. D. Genetics of scapula and pelvis development: an evolutionary perspective. *Curr. Top. Dev. Biol.* **132**, 311–349 (2019).

Acknowledgements

We thank A. Gillis for kindly sharing elephant shark tissue. J. Lemberg provided technical assistance for μ CT scanning and analysis. We thank N.H. Shubin for providing fish space, A.A. Abbasi for providing the PXIG vector, G. Senevirathne for sharing the HCR protocol, Y.J. Chang and Office of Advanced Research Computing Rutgers for computational assistance, J.J. Tena for visualization of high-throughput sequencing results, D. Remsen, S. Bennett, and staffs at the Marine Resource Center at MBL for skate embryos, J. Talbot for technical advice of live fluorescent imaging, G. Crump and C. Arata for sharing osteoblast and chondrocyte fluorescence transgenic fish, the Bayosphere Lab (A. Ferrara) at Nicholls State University for help with gar sampling, and Brett Racicot (Michigan State University) for gar husbandry. We thank M.B. Hawkins for providing critical comments to the manuscript. This work was performed with Honors College with Johnson & Johnson Women in STEM2D Life Sciences Summer Undergraduate Research Fellowship (to J.W.), The Paul Robeson Scholarship, the Enrico P. Veltri Scholarship for the Life Sciences, Duncan and Nancy MacMillan Award for Research Excellence (to T.W.), the Division of Life Sciences Summer Undergraduate Research Fellowship provided by Macmillan foundation (to A.S.), The INSPIRE program (IRACDA New Jersey/New York for Science Partnerships in Research & Education) (to D.N.), NSF EDGE grant 2029216 (to I.B.), the institutional support provided by the Rutgers University School of Arts and Sciences and the Human Genetics Institute of New Jersey, the National Science Foundation under Grant IOS 2210072, Marine Biological Laboratory Whitman Fellowship (2018), Society for Developmental Biology Innovation Grant (2020), and Busch Biomedical Grant (to T.N.).

Author contributions

T.W., I.B., and T.N. designed research. K.F. and T.N. created genetically modified fish. J.W., A.S., and T.N. analyzed RNA-sequencing data, ATAC-sequencing data, and conducted chromogenic whole mount in situ hybridization and HCR. A.E., A.A., K.F., D.B., and H.C. genotyped transgenic and knockout fish. T.S. and T.N. conducted CT scan. T.W. created

pectoral girdle bone 3D reconstructions from CT scan data. I.B. and O.F. conducted phylogenetic and synteny analyses and spotted gar in situ hybridization. D.G. conducted statistical analyses. S.A. conducted CT analysis of the telencephalon. D.N. conducted in situ hybridization of skate embryos. T.W., J.W., and T.N. analyzed the data. S.K., T.S., I.B., and T.N. wrote the paper.

Competing interests

The authors declare no competing interests.

Additional information

Supplementary information The online version contains supplementary material available at <https://doi.org/10.1038/s41467-025-60236-z>.

Correspondence and requests for materials should be addressed to Tetsuya Nakamura.

Peer review information *Nature Communications* thanks Sarah K McMenamin and the other anonymous reviewer(s) for their contribution to the peer review of this work. A peer review file is available.

Reprints and permissions information is available at <http://www.nature.com/reprints>

Publisher's note Springer Nature remains neutral with regard to jurisdictional claims in published maps and institutional affiliations.

Open Access This article is licensed under a Creative Commons Attribution-NonCommercial-NoDerivatives 4.0 International License, which permits any non-commercial use, sharing, distribution and reproduction in any medium or format, as long as you give appropriate credit to the original author(s) and the source, provide a link to the Creative Commons licence, and indicate if you modified the licensed material. You do not have permission under this licence to share adapted material derived from this article or parts of it. The images or other third party material in this article are included in the article's Creative Commons licence, unless indicated otherwise in a credit line to the material. If material is not included in the article's Creative Commons licence and your intended use is not permitted by statutory regulation or exceeds the permitted use, you will need to obtain permission directly from the copyright holder. To view a copy of this licence, visit <http://creativecommons.org/licenses/by-nc-nd/4.0/>.

© The Author(s) 2025